Standard Reference Materials:

Description of the SRM 1965 Microsphere Slide

A. W. Hartman
Precision Engineering Division
National Engineering Laboratory
National Institute of Standards and Technology
Gaithersburg, MD 20899

and

R. L. McKenzie
Office of Standard Reference Materials
National Measurement Laboratory
National Institute of Standards and Technology
Gaithersburg, MD 20899

NOTE: As of 23 August 1988, the National Bureau of Standards (NBS) became the National Institute of Standards and Technology (NIST) when President Reagan signed into law the Omnibus Trade and Competitiveness Act.

U.S. DEPARTMENT OF COMMERCE, C. William Verity, Secretary
NATIONAL INSTITUTE OF STANDARDS AND TECHNOLOGY, Ernest Ambler, Director
(formerly National Bureau of Standards)

Issued November 1988

Library of Congress Catalog Card Number: 88–600598
National Institute of Standards and Technology
Special Publication 260-107, 67 pages (Nov. 1988)

U.S. GOVERNMENT PRINTING OFFICE
WASHINGTON: 1988

For sale by the Superintendent of Documents, U.S. Government Printing Office, Washington, DC 20402–9325

Preface

Standard Reference Materials (SRM's) as defined by the National Institute of Standards and Technology (NIST) are well-characterized materials, produced in quantity and certified for one or more physical or chemical properties. They are used to assure the accuracy and compatibility of measurements throughout the Nation. SRM's are widely used as primary standards in many diverse fields in science, industry, and technology, both within the United States and throughout the world. They are also used extensively in the fields of environmental and clinical analysis. In many applications, traceability of quality control and measurement processes to the national measurement system is carried out through the mechanism and use of SRM's. For many of the Nation's scientists and technologists, it is therefore of more than passing interest to know the details of the measurements made at NIST in arriving at the certified values of the SRM's produced. An NIST series of papers, of which this publication is a member, called the NIST Special Publication - 260 Series, is reserved for this purpose.

The 260 Series is dedicated to the dissemination of information on different phases of the preparation, measurement, certification, and use of NIST SRM's. In general, much more detail will be found in these papers than is generally allowed, or desirable, in scientific journal articles. This enables the user to assess the validity and accuracy of the measurement processes employed, to judge the statistical analysis, and to learn details of techniques and methods utilized for work entailing greatest care and accuracy. These papers also should provide sufficient additional information not found on the certificate so that new applications in diverse fields not foreseen at the time the SRM was originally issued will be sought and found.

Inquiries concerning the technical content of this paper should be directed to the author(s). Other questions concerned with the availability, delivery, price, and so forth, will receive prompt attention from:

Office of Standard Reference Materials
National Institute of Standards and Technology
Gaithersburg, MD 20899

Stanley D. Rasberry, Chief
Office of Standard Reference Materials

OTHER NIST PUBLICATIONS IN THIS SERIES

Seward, R. W., ed., NBS Standard Reference Materials Catalog 1988-89, NBS Spec. Publ. 260 (January 1988)

Michaelis, R. E., and Wyman, L. L., Standard Reference Materials: Preparation of White Cast Iron Spectrochemical Standards, NBS Misc. Publ. 260-1 (June 1964). COM74-11061**

Michaelis, R. E., Wyman, L. L., and Flitsch, R., Standard Reference Materials: Preparation of NBS Copper-Base Spectrochemical Standards, NBS Misc. Publ. 260-2 (October 1964). COM74-11063**

Michaelis, R. E., Yakowitz, H., and Moore, G. A., Standard Reference Materials: Metallographic Characterization of an NBS Spectrometric Low-Alloy Steel Standard, NBS Misc. Publ. 260-3 (October 1964). COM74-11060**

Alvarez, R., and Flitsch, R., Standard Reference Materials: Accuracy of Solution X-Ray Spectrometric Analysis of Copper-Base Alloys, NBS Misc. Publ. 260-5 (March 1965). PB168068**

Shultz, J. I., Standard Reference Materials: Methods for the Chemical Analysis of White Cast Iron Standards, NBS Misc. Publ. 260-6 (July 1965). COM74-11068**

Bell, R. K., Standard Reference Materials: Methods for the Chemical Analysis of NBS Copper-Base Spectrochemical Standards, NBS Misc. Publ. 260-7 (October 1965). COM74-11067**

Richmond, M. S., Standard Reference Materials: Analysis of Uranium Concentrates at the National Bureau of Standards, NBS Misc. Publ. 260-8 (December 1965). COM74-11066**

Anspach, S. C., Cavallo, L. M., Garfinkel, S. B., Hutchinson, J. M. R., and Smith, C. N., Standard Reference Materials: Half Lives of Materials Used in the Preparation of Standard Reference Materials of Nineteen Radioactive Nuclides Issued by the National Bureau of Standards, NBS Misc. Publ. 260-9 (November 1965). COM74-11065**

Yakowitz, H., Vieth, D. L., Heinrich, K. F. J., and Michaelis, R. E., Standard Reference Materials: Homogeneity Characterization of NBS Spectrometric Standards II: Cartridge Brass and Low-Alloy Steel, NBS Misc. Publ. 260-10 (December 1965). COM74-11064**

Napolitano, A., and Hawkins, E. G., Standard Reference Materials: Viscosity of Standard Lead-Silica Glass, NBS Misc. Publ. 260-11 (November 1966).

Yakowitz, H., Vieth, D. L., and Michaelis, R. E., Standard Reference Materials: Homogeneity Characterization of NBS Spectrometric Standards III: White Cast Iron and Stainless Steel Powder Compact, NBS Misc. Publ. 260-12 (September 1966).

Menis, O., and Sterling, J. T., Standard Reference Materials: Determination of Oxygen in Ferrous Materials—SRM 1090, 1091, and 1092, NBS Misc. Publ. 260-14 (September 1966).

Yakowitz, H., Michaelis, R. E., and Vieth, D. L., Standard Reference Materials: Homogeneity Characterization of NBS Spectrometric Standards IV: Preparation and Microprobe Characterization of W-20% Mo Alloy Fabricated by Powder Metallurgical Methods, NBS Spec. Publ. 260-16 (January 1969). COM74-11062**

Paule, R. C., and Mandel, J., Standard Reference Materials: Analysis of Interlaboratory Measurements on the Vapor Pressure of Gold (Certification of Standard Reference Material 745). NBS Spec. Publ. 260-19 (January 1970). PB190071**

Paule, R. C., and Mandel, J., Standard Reference Materials: Analysis of Interlaboratory Measurements on the Vapor Pressures of Cadmium and Silver, NBS Spec. Publ. 260-21 (January 1971). COM74-11359**

Yakowitz, H., Fiori, C. E., and Michaelis, R. E., Standard Reference Materials: Homogeneity Characterization of Fe-3 Si Alloy, NBS Spec. Publ. 260-22 (February 1971). COM74-11357**

Napolitano, A., and Hawkins, E. G., Standard Reference Materials: Viscosity of a Standard Borosilicate Glass, NBS Spec. Publ. 260-23 (December 1970). COM71-00157**

Sappenfield, K. M., Marinenko, G., and Hague, J. L., Standard Reference Materials: Comparison of Redox Standards, NBS Spec. Publ. 260-24 (January 1972). COM72-50058**

Hicho, G. E., Yakowitz, H., Rasberry, S. D., and Michaelis, R. E., Standard Reference Materials: A Standard Reference Material Containing Nominally Four Percent Austenite, NBS Spec. Publ. 260-25 (February 1971). COM74-11356**

Martin, J. F., Standard Reference Materials: National Bureau of Standards-US Steel Corporation Joint Program for Determining Oxygen and Nitrogen in Steel, NBS Spec. Publ. 260-26 (February 1971). PB 81176620**

Garner, E. L., Machlan, L. A., and Shields, W. R., Standard Reference Materials: Uranium Isotopic Standard Reference Materials, NBS Spec. Publ. 260-27 (April 1971). COM74-11358**

Heinrich, K. F. J., Myklebust, R. L., Rasberry, S. D., and Michaelis, R. E., Standard Reference Materials: Preparation and Evaluation of SRM's 481 and 482 Gold-Silver and Gold-Copper Alloys for Microanalysis, NBS Spec. Publ. 260-28 (August 1971). COM71-50365**

Geller, S. B., Standard Reference Materials: Calibration of NBS Secondary Standard Magnetic Tape (Computer Amplitude Reference) Using the Reference Tape Amplitude Measurement "Process A-Model 2," NBS Spec. Publ. 260-29 (June 1971). COM71-50282**

Gorozhanina, R. S., Freedman, A. Y., and Shaievitch, A. B. (translated by M. C. Selby), Standard Reference Materials: Standard Samples Issued in the USSR (A Translation from the Russian), NBS Spec. Publ. 260-30 (June 1971). COM71-50283**

Hust, J. G., and Sparks, L. L., Standard Reference Materials: Thermal Conductivity of Electrolytic Iron SRM 734 from 4 to 300 K, NBS Spec. Publ. 260-31 (November 1971). COM71-50563**

Mavrodineanu, R., and Lazar, J. W., Standard Reference Materials: Standard Quartz Cuvettes for High Accuracy Spectrophotometry, NBS Spec. Publ. 260-32 (December 1973). COM74-50018**

Wagner, H. L., Standard Reference Materials: Comparison of Original and Supplemental SRM 705, Narrow Molecular Weight Distribution Polystyrene, NBS Spec. Publ. 260-33 (May 1972). COM72-50526**

Sparks, L. L., and Hust, J. G., Standard Reference Materials: Thermal Conductivity of Austenitic Stainless Steel, SRM 735 from 5 to 280 K, NBS Spec. Publ. 260-35 (April 1972.) COM72-50368**

Cali, J. P., Mandel, J., Moore, L. J., and Young, D. S., Standard Reference Materials: A Referee Method for the Determination of Calcium in Serum NBS SRM 915, NBS Spec. Publ. 260-36 (May 1972). COM72-50527**

Shultz, J. I., Bell, R. K., Rains, T. C., and Menis, O., Standard Reference Materials: Methods of Analysis of NBS Clay Standards, NBS Spec. Publ. 260-37 (June 1972). COM72-50692**

Clark, A. F., Denson, V. A., Hust, J. G., and Powell, R. L., Standard Reference Materials: The Eddy Current Decay Method for Resistivity Characterization of High-Purity Metals, NBS Spec. Publ. 260-39 (May 1972). COM72-50529**

McAdie, H. G., Garn, P. D., and Menis, O., Standard Reference Materials: Selection of Thermal Analysis Temperature Standards Through a Cooperative Study (SRM 758, 759, 760), NBS Spec. Publ. 260-40 (August 1972) COM72-50776**

Wagner, H. L., and Verdier, P. H., eds., Standard Reference Materials: The Characterization of Linear Polyethylene, SRM 1475, NBS Spec. Publ. 260-42 (September 1972). COM72-50944**

Yakowitz, H., Ruff, A. W., and Michaelis, R. E., Standard Reference Materials: Preparation and Homogeneity Characterization of an Austenitic Iron-Chromium-Nickel Alloy, NBS Spec. Publ. 260-43 (November 1972). COM73-50760**

Schooley, J. F., Soulen, R. J., Jr., and Evans, G. A., Jr., Standard Reference Materials: Preparation and Use of Superconductive Fixed Point Devices, SRM 767, NBS Spec. Publ. 260-44 (December 1972). COM73-50037**

Greifer, B., Maienthal, E. J., Rains, T. C., and Rasberry, S. D., Standard Reference Materials: Powdered Lead-Based Paint, SRM 1579, NBS Spec. Publ. 260-45 (March 1973). COM73-50226**

Hust, J. G., and Giarratano, P. J., Standard Reference Materials: Thermal Conductivity and Electrical Resistivity Standard Reference Materials: Austenitic Stainless Steel, SRM's 735 and 798, from 4 to 1200 K, NBS Spec. Publ. 260-46 (March 1975). COM75-10339**

Hust, J. G., Standard Reference Materials: Electrical Resistivity of Electrolytic Iron, SRM 797, and Austenitic Stainless Steel, SRM 798, from 5 to 280 K, NBS Spec. Publ. 260-47 (February 1974). COM74-50176**

Mangum, B. W., and Wise, J. A., Standard Reference Materials: Description and Use of Precision Thermometers for the Clinical Laboratory, SRM 933 and SRM 934, NBS Spec. Publ. 260-48 (May 1974). COM74-50533**

Carpenter, B. S., and Reimer, G. M., Standard Reference Materials: Calibrated Glass Standards for Fission Track Use, NBS Spec. Publ. 260-49 (November 1974). COM74-51185**

Hust, J. G., and Giarratano, P. J., Standard Reference Materials: Thermal Conductivity and Electrical Resistivity Standard Reference Materials: Electrolytic Iron, SRM's 734 and 797 from 4 to 1000 K, NBS Spec. Publ. 260-50 (June 1975). COM75-10698**

Mavrodineanu, R., and Baldwin, J. R., Standard Reference Materials: Glass Filters As a Standard Reference Material for Spectrophotometry-Selection, Preparation, Certification, Use-SRM 930 NBS Spec. Publ. 260-51 (November 1975). COM75-10339**

Hust, J. G., and Giarratano, P. J., Standard Reference Materials: Thermal Conductivity and Electrical Resistivity Standard Reference Materials 730 and 799, from 4 to 3000 K, NBS Spec. Publ. 260-52 (September 1975). COM75-11193**

Durst, R. A., Standard Reference Materials: Standardization of pH Measurements, NBS Spec. Publ. 260-53 (February 1988, Revision of December 1975 version).

Burke, R. W., and Mavrodineanu, R., Standard Reference Materials: Certification and Use of Acidic Potassium Dichromate Solutions as an Ultraviolet Absorbance Standard, NBS Spec. Publ. 260-54 (August 1977). PB272168**

Ditmars, D. A., Cezairliyan, A., Ishihara, S., and Douglas, T. B., Standard Reference Materials: Enthalpy and Heat Capacity; Molybdenum SRM 781, from 273 to 2800 K, NBS Spec. Publ. 260-55 (September 1977). PB272127**

Powell, R. L., Sparks, L. L., and Hust, J. G., Standard Reference Materials: Standard Thermocouple Material, Pt-67: SRM 1967, NBS Spec. Publ. 260-56 (February 1978). PB277172**

Barnes, J. D., and Martin, G. M., Standard Reference Materials: Polyester Film for Oxygen Gas Transmission Measurements SRM 1470, NBS Spec. Publ. 260-58 (June 1979). PB297098**

Velapoldi, R. A., Paule, R. C., Schaffer, R., Mandel, J., and Moody, J. R., Standard Reference Materials: A Reference Method for the Determination of Sodium in Serum, NBS Spec. Publ. 260-60 (August 1978). PB286944**

Verdier, P H., and Wagner, H. L., Standard Reference Materials: The Characterization of Linear Polyethylene (SRM 1482, 1483, 1484), NBS Spec. Publ. 260-61 (December 1978). PB289899**

Soulen, R. J., and Dove, R. B., Standard Reference Materials: Temperature Reference Standard for Use Below 0.5 K (SRM 768), NBS Spec. Publ. 260-62 (April 1979). PB294245**

Velapoldi, R. A., Paule, R. C., Schaffer, R., Mandel, J., Machlan, L. A., and Gramlich, J. W., Standard Reference Materials: A Reference Method for the Determination of Potassium in Serum, NBS Spec. Publ. 260-63 (May 1979). PB297207**

Velapoldi, R. A., and Mielenz, K. D., Standard Reference Materials: A Fluorescence Standard Reference Material Quinine Sulfate Dihydrate (SRM 936), NBS Spec. Publ. 260-64 (January 1980). PB80-132046**

Marinenko, R. B., Heinrich, K. F. J., and Ruegg, F. C., Standard Reference Materials: Micro-Homogeneity Studies of NBS Standard Reference Materials, NBS Research Materials, and Other Related Samples, NBS Spec. Publ. 260-65 (September 1979). PB300461**

Venable, W. H., Jr., and Eckerle, K. L., Standard Reference Materials: Didymium Glass Filters for Calibrating the Wavelength Scale of Spectrophotometers-SRM 2009, 2010, 2013, and 2014, NBS Spec. Publ. 260-66 (October 1979). PB80-104961**

Velapoldi, R. A., Paule, R. C., Schaffer, R., Mandel, J., Murphy, T. J., and Gramlich, J. W., Standard Reference Materials: A Reference Method for the Determination of Chloride in Serum, NBS Spec. Publ. 260-67 (November 1979). PB80-110117**

Mavrodineanu, R., and Baldwin, J. R., Standard Reference Materials: Metal-On-Quartz Filters as a Standard Reference Material for Spectrophotometry SRM 2031, NBS Spec. Publ. 260-68 (April 1980). PB80-197486**

Velapoldi, R. A., Paule, R. C., Schaffer, R., Mandel, J., Machlan, L. A., Garner, E. L., and Rains, T. C., Standard Reference Materials: A Reference Method for the Determination of Lithium in Serum, NBS Spec. Publ. 260-69 (July 1980). PB80-209117**

Marinenko, R. B., Biancaniello, F., Boyer, P. A., Ruff, A. W., and DeRobertis, L., Standard Reference Materials: Preparation and Characterization of an Iron-Chromium-Nickel Alloy for Microanalysis, NBS Spec. Publ. 260-70 (May 1981). PB84-165349**

Seward, R. W., and Mavrodineanu, R., Standard Reference Materials: Summary of the Clinical Laboratory Standards Issued by the National Bureau of Standards, NBS Spec. Publ. 260-71 (November 1981). PB82-135161**

Reeder, D. J., Coxon, B., Enagonio, D., Christensen, R. G., Schaffer, R., Howell, B. F., Paule, R. C., and Mandel, J., Standard Reference Materials: SRM 900, Antiepilepsy Drug Level Assay Standard, NBS Spec. Publ. 260-72 (June 1981). PB81-220758

Interrante, C. G., and Hicho, G. E., Standard Reference Materials: A Standard Reference Material Containing Nominally Fifteen Percent Austenite (SRM 486), NBS Spec. Publ. 260-73 (January 1982). PB82-215559**

Marinenko, R. B., Standard Reference Materials: Preparation and Characterization of K-411 and K-414 Mineral Glasses for Microanalysis: SRM 470, NBS Spec. Publ. 260-74 (April 1982). PB82-221300**

Weidner, V. R., and Hsia, J. J., Standard Reference Materials: Preparation and Calibration of First Surface Aluminum Mirror Specular Reflectance Standards (SRM 2003a), NBS Spec. Publ. 260-75 (May 1982). PB82-221367**

Hicho, G. E., and Eaton, E. E., Standard Reference Materials: A Standard Reference Material Containing Nominally Five Percent Austenite (SRM 485a), NBS Spec. Publ. 260-76 (August 1982). PB83-115568**

Furukawa, G. T., Riddle, J. L., Bigge, W. G., and Pfieffer, E. R., Standard Reference Materials: Application of Some Metal SRM's as Thermometric Fixed Points, NBS Spec. Publ. 260-77 (August 1982). PB83-117325**

Hicho, G. E., and Eaton, E. E., Standard Reference Materials: Standard Reference Material Containing Nominally Thirty Percent Austenite (SRM 487), NBS Spec. Publ. 260-78 (September 1982). PB83-115576**

Richmond, J. C., Hsia, J. J., Weidner, V. R., and Wilmering, D. B., Standard Reference Materials: Second Surface Mirror Standards of Specular Spectral Reflectance (SRM's 2023, 2024, 2025), NBS Spec. Publ. 260-79 (October 1982). PB84-203447**

Schaffer, R., Mandel, J., Sun, T., Cohen, A., and Hertz, H. S., Standard Reference Materials: Evaluation by an ID/MS Method of the AACC Reference Method for Serum Glucose, NBS Spec. Publ. 260-80 (October 1982). PB84-216894**

Burke, R. W., and Mavrodineanu, R., Standard Reference Materials: Accuracy in Analytical Spectrophotometry, NBS Spec. Publ. 260-81 (April 1983). PB83-214536**

Weidner, V. R., Standard Reference Materials: White Opal Glass Diffuse Spectral Reflectance Standards for the Visible Spectrum (SRM's 2015 and 2016), NBS Spec. Publ. 260-82 (April 1983). PB83-220723**

Bowers, G. N., Jr., Alvarez, R., Cali, J. P., Eberhardt, K. R., Reeder, D. J., Schaffer, R., and Uriano, G. A., Standard Reference Materials: The Measurement of the Catalytic (Activity) Concentration of Seven Enzymes in NBS Human Serum SRM 909, NBS Spec. Publ. 260-83 (June 1983). PB83-239509**

Gills, T. E., Seward, R. W., Collins, R. J., and Webster, W. C., Standard Reference Materials: Sampling, Materials Handling, Processing, and Packaging of NBS Sulfur in Coal Standard Reference Materials 2682, 2683, 2684, and 2685, NBS Spec. Publ. 260-84 (August 1983). PB84-109552**

Swyt, D. A., Standard Reference Materials: A Look at Techniques for the Dimensional Calibration of Standard Microscopic Particles, NBS Spec. Publ. 260-85 (September 1983). PB84-112648**

Hicho, G. E., and Eaton, E. E., Standard Reference Materials: A Standard Reference Material Containing Two and One-Half Percent Austenite, SRM 488, NBS Spec. Publ. 260-86 (December 1983). PB84-143296**

Mangum, B. W., Standard Reference Materials: SRM 1969: Rubidium Triple-Point - A Temperature Reference Standard Near 39.30 °C, NBS Spec. Publ. 260-87 (December 1983). PB84-149996**

Gladney, E. S., Burns, C. E., Perrin, D. R., Roelandts, I., and Gills, T. E., Standard Reference Materials: 1982 Compilation of Elemental Concentration Data for NBS Biological, Geological, and Environmental Standard Reference Materials, NBS Spec. Publ. 260-88 (March 1984). PB84-218338**

Hust, J. G., Standard Reference Materials: A Fine-Grained, Isotropic Graphite for Use as NBS Thermophysical Property RM's from 5 to 2500 K, NBS Spec. Publ. 260-89 (September 1984). PB85-112886**

Hust, J. G., and Lankford, A. B., Standard Reference Materials: Update of Thermal Conductivity and Electrical Resistivity of Eleetrolytic Iron, Tungsten, and Stainless Steel, NBS Spec. Publ. 260-90 (September 1984). PB85-115814**

Goodrich, L. F., Vecchia, D. F., Pittman, E. S., Ekin, J. W., and Clark, A. F., Standard Reference Materials: Critical Current Measurements on an NbTi Superconducting Wire Standard Reference Material, NBS Spec. Publ. 260-91 (September 1984). PB85-118594**

Carpenter, B. S., Standard Reference Materials: Calibrated Glass Standards for Fission Track Use (Supplement to NBS Spec. Publ. 260-49), NBS Spec. Publ. 260-92 (September 1984). PB85-113025**

Ehrstein, J.R., Standard Reference Materials: Preparation and Certification of Standard Reference Materials for Calibration of Spreading Resistance Probes, NBS Spec. Publ. 260-93 (January 1985). PB85-177921**

Gills, T. E., Koch, W. F., Stolz, J. W., Kelly, W. R., Paulsen, P. J., Colbert, J. C., Kirklin, D. R., Pei, P.T.S., Weeks, S., Lindstrom, R. M., Fleming, R. F., Greenberg, R. R., and Paule, R. C., Standard Reference Materials: Methods and Procedures Used at the National Bureau of Standards to Certify Sulfur in Coal SRM's for Sulfur Content, Calorific Value, Ash Content, NBS Spec. Publ. 260-94 (December 1984). PB85-165900**

Mulholland, G. W., Hartman, A. W., Hembree, G. G., Marx, E., and Lettieri, T. R., Standard Reference Materials: Development of a 1 μm Diameter Particle Size Standard, SRM 1690, NBS Spec. Publ. 260-95 (May 1985). SN003-003-02665-4*

Carpenter, B. S., Gramlich, J. W., Greenberg, R. R., Machlan, L. A., DeBievre, P., Eschbach, H. L., Meyer, H., Van Audenhove, J., Connolly, V. E., Trahey, N. M., and Zook, A. C., Standard Reference Materials: Uranium-235 Isotopic Abundance Standard Reference Materials for Gamma Spectrometry Measurements, NBS Spec. Publ. 260-96 (September 1986). PB87-108544**

Mavrodineanu, R., and Gills, T. E., Standard Reference Materials: Summary of the Coal, Ore, Mineral, Rock, and Refactory Standards Issued by the National Bureau of Standards, NBS Spec. Publ. 260-97 (September 1985). SN003-003-02688-3*

Hust, J. G., Standard Reference Materials: Glass Fiberboard SRM for Thermal Resistance, NBS Spec. Publ. 260-98 (August 1985). SN003-003-02674-3*

Callanan, J. E., Sullivan, S. A., and Vecchia, D. F., Standard Reference Materials: Feasibility Study for the Development of Standards Using Differential Scanning Calorimetry, NBS Spec. Publ. 260-99 (August 1985). SN003-003-02675-1*

Taylor, J. K., Standard Reference Materials: Handbook for SRM Users, NBS Spec. Publ. 260-100 (September 1985). PB86-110897**

Mangum, B. W., Standard Reference Materials: SRM 1970, Succinonitrile Triple-Point Standard: A Temperature Reference Standard Near 58.08 °C, NBS Spec. Publ. 260-101 (March 1986). SN003-003-02722-7*

Weidner, V. R., Mavrodineanu, R., Mielenz, K. D., Velapoldi, R. A., Eckerle, K. L., and Adams, B., Standard Reference Materials: Holmium Oxide Solution Wavelength Standard from 240 to 640 nm - SRM 2034, NBS Spec. Publ. 260-102 (July 1986). PB86-245727**

Hust, J. G., Standard Reference Materials: Glass Fiberblanket SRM for Thermal Resistance, NBS Spec. Publ. 260-103 (September 1985). SN003-003-02687-5*

Mavrodineanu, R., and Alvarez, R., Standard Reference Materials: Summary of the Biological and Botanical Standards Issued by the National Bureau of Standards, NBS Spec. Publ. 260-104 (November 1985). SN003-003-02704-9*

Mavrodineanu, R., and Rasberry, S. D., Standard Reference Materials: Summary of the Environmental Research, Analysis, and Control Standards Issued by the National Bureau of Standards, NBS Spec. Publ. 260-105 (March 1986). SN003-003-02725-1*

Koch, W. F., ed., Standard Reference Materials: Methods and Procedures Used at the National Bureau of Standards to Prepare, Analyze, and Certify SRM 2694, Simulated Rainwater, and Recommendations for Use, NBS Spec. Publ. 260-106 (July 1986). PB86-247483**

Hartman, A. W., and McKenzie, R. L., Standard Reference Materials: SRM 1965, Microsphere Slide (10 μm Polystyrene Spheres), NBS Spec. Publ. 260-107 (In Preparation).

Mavrodineanu, R., and Gills, T. E., Standard Reference Materials: Summary of Gas Cylinder and Permeation Tube Standard Reference Materials Issued by the National Bureau of Standards, NBS Spec. Publ. 260-108 (May 1987).

Candela, G. A., Chandler-Horowitz, D., Novotny, D. B., Marchiando, J. F., and Belzer, B. J., Standard Reference Materials: Preparation and Certification of an Ellipsometrically Derived Thickness and Refractive Index Standard of a Silicon Dioxide Film (SRM 2530), NIST Spec. Publ. 260-109 (October 1988).

Kirby, R. K., and Kanare, H. M., Standard Reference Materials: Portland Cement Chemical Composition Standards (Blending, Packaging, and Testing), NBS Spec. Publ. 260-110 (February 1988).

Gladney, E. S., O'Malley, B. T., Roelandts, I., and Gills, T. E., Standard Reference Materials: Compilation of Elemental Concentration Data for NBS Clinical, Biological, Geological, and Environmental Standard Reference Materials, NBS Spec. Publ. 260-111 (November 1987).

*Send order with remittance to Superintendent of Documents, U.S. Government Printing Office, Washington, DC 20102. Remittance from foreign countries should include an additional one fourth of the purchase price for postage.

**May be ordered from: National Technical Information Services (NTIS), Springfield, VA 22161.

DESCRIPTION OF THE SRM 1965 MICROSPHERE SLIDE

A. W. Hartman
Precision Engineering Division

and R. L. McKenzie
Office of Standard Reference Materials

Table of Contents

List of Figures

1. INTRODUCTION AND OVERVIEW

This report describes the construction, preparation, and recommended uses of the microsphere slide. The preparation material consists of monosize polystyrene microspheres with a Gaussian diameter distribution characterized by a mean diameter, $\bar{D}$, of 9.89 ± 0.04 μm and a standard deviation, σ_D, of 0.09 ± 0.01 μm. This material was made under conditions of microgravity during several NASA space shuttle flights, and is available from NIST (formerly NBS) as a Standard Reference Material for particle size (SRM 1960). The size distribution is narrow, and the sphericity is very good. Its dimensional calibration was at the time (1985) the most accurate microsphere particle calibration done at NBS.

The microsphere material has been deposited as fixed, two-dimensional, close-packed structures, permanently sealed on a microscope slide. The dimensional information that these slides contain is offered to microscopists as a measurement tool, and to teachers and students for purposes of teaching and studying aspects of micrometrology and crystallography.

In Section 2 the Microsphere Slide is briefly described. Its use as a measurement tool is discussed in Section 3, several educational uses for the slide are given in Section 4 and a description of how the slide was made is given in Section 5. The Appendix contains reprints of two papers describing various experiments of materials processing under conditions of microgravity and the details of the production of the monodisperse polystyrene microspheres aboard the space shuttle.

2. DESCRIPTION OF THE SRM 1965 MICROSPHERE SLIDE

The slide contains two separate groupings of microspheres. In one area the sphere grouping is ordered in two-dimensional hexagonal arrays, in the other area the sphere grouping is unordered and resembles strings of beads in contact. Examples of each type of grouping are shown in Figure 1.

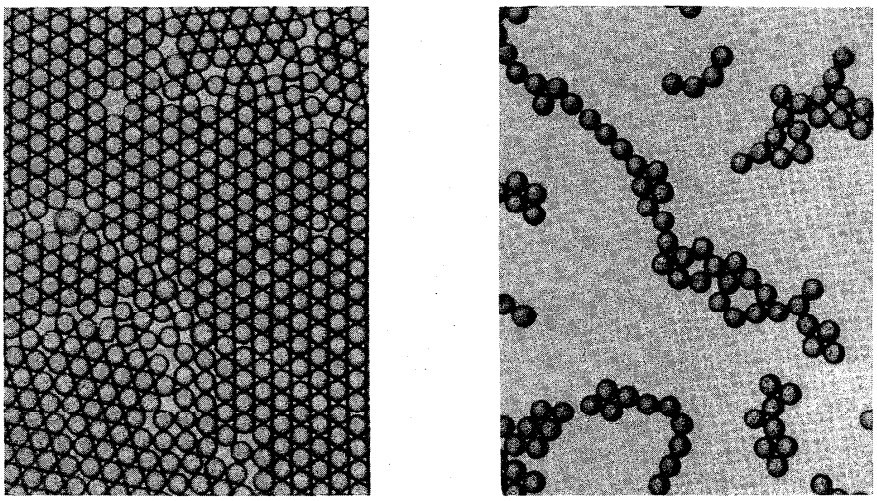

Figure 1. Close-packed microsphere structures.

The spheres are permanently sealed in an air chamber, formed by the microscope slide as a flat substrate, a cover glass with central hole defining the sphere deposition area and forming the chamber cavity, and a second cover glass sealing the chamber and protecting the microsphere structures (Fig. 2).

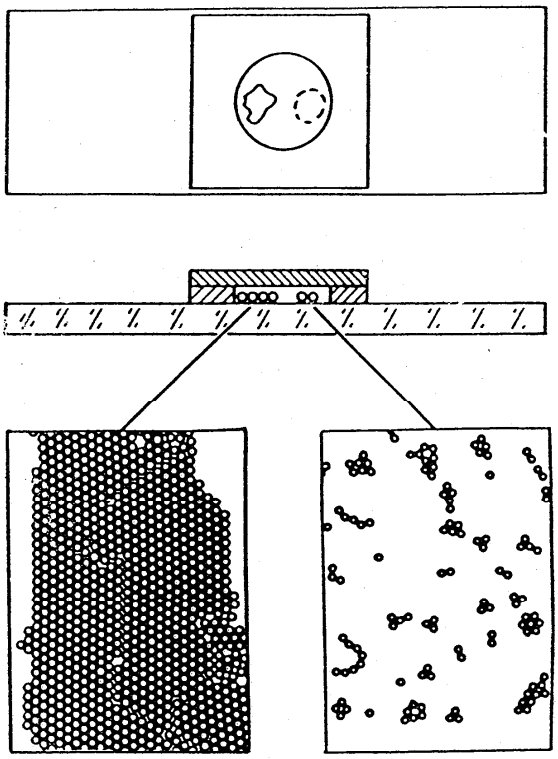

The microsphere material is the same as that used in NIST Standard Reference Material SRM 1960 – polystyrene spheres with a Gaussian diameter distribution, characterized by mean diameter, $\bar{D}$, of 9.84 ± 0.04 μm and a standard deviation, σ_D, of 0.09 ± 0.01 μm.

Figure 2. Diagram of the Microsphere Slide.

3. THE MICROSPHERE SLIDE AS A MEASUREMENT TOOL

The slide carries microscopic spheres of nominally equal and statistically known size; it can therefore serve as a ruler or length standard of microscopic dimensions. It can be used in the calibration of microlength measuring instruments or procedures that utilize optical microscopes, including the determination of image magnification and image distortion of the microscope itself. In this section a number of uses will be described of the Microsphere Slide as a measurement tool.

3.1 A microlength scale

The ordered microsphere grouping on the slide contains many hexagonal arrays which consist of rows of almost equal-size spheres. A microsphere row can be considered a microlength scale, each scale division being one sphere diameter in length.

The length of a row can be read by sighting the sphere centers or the contact areas between spheres, using an eyepiece micrometer scale or crosshairs. The resolution of this readout process is typically 5% – 10% of a sphere diameter (0.5 – 1 μm). The scale divisions can be made to look sharper by stopping the microscope condensor way down (or taking it out), allowing almost parallel light to illuminate the microsphere area. Because each sphere is transparent, it acts as a spherical lens, refracting the parallel incoming light into a small focal spot just above each sphere. If the microscope is refocused onto the common back-focal plane of the spheres, rows of small and equispaced focal spots will appear in the field of view as bright points of light (see Fig. 3).

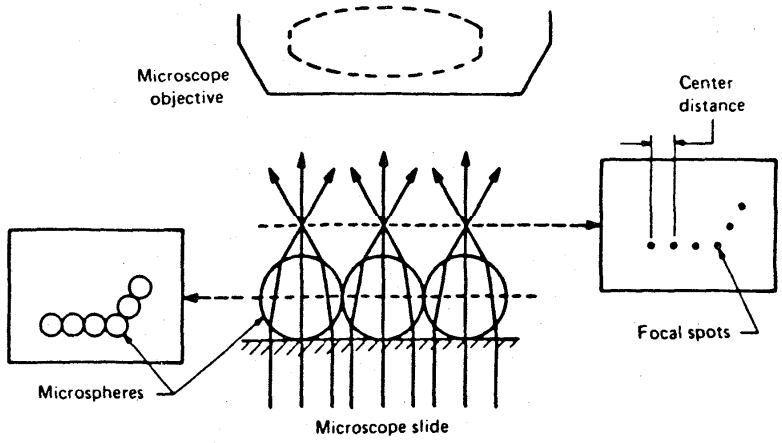

Figure 3. Parallel illumination producing focal spots.

These focal spots, which mark the sphere centers in the field or on a photomicrograph, are circular, uniform, and much smaller that the spheres themselves. A ray trace for a polystyrene sphere, illuminated by parallel blue-green light and viewed by a 0.50 NA microscope objective, predicts that the focal spots have a diameter of 0.03 D where D is the sphere diameter. For spheres smaller than about 20 μm the focal spot diameter becomes equal to that of an Airy diffraction disk (1.2λ/NA, or 1 μm for 10-μm spheres). Examples are shown in Figure 4. It is thus possible to realize a microscopic scale or ruler, consisting of a row of equispaced focal spots as in Figure 5, in which each scale division can be read out with very high resolution.

The diameter of each sphere in the microsphere scale is known only statistically, therefore the scale accuracy goes up in relative terms as the number of spheres in the scale increases. The minimum scale length is 10 μm , the maximum is 100 – 200 μm depending on the available array row lengths on the microsphere slide and on the field of view.

It is possible to increase the relative accuracy of the scale beyond that of the longest available microsphere row by including several neighboring rows. In this way ordered assemblies containing 100 and more spheres can be used. For instance, a 10 × 10 array can define the image magnification at the array image area in the film plane with an accuracy close to 0.5%, as will be shown below.

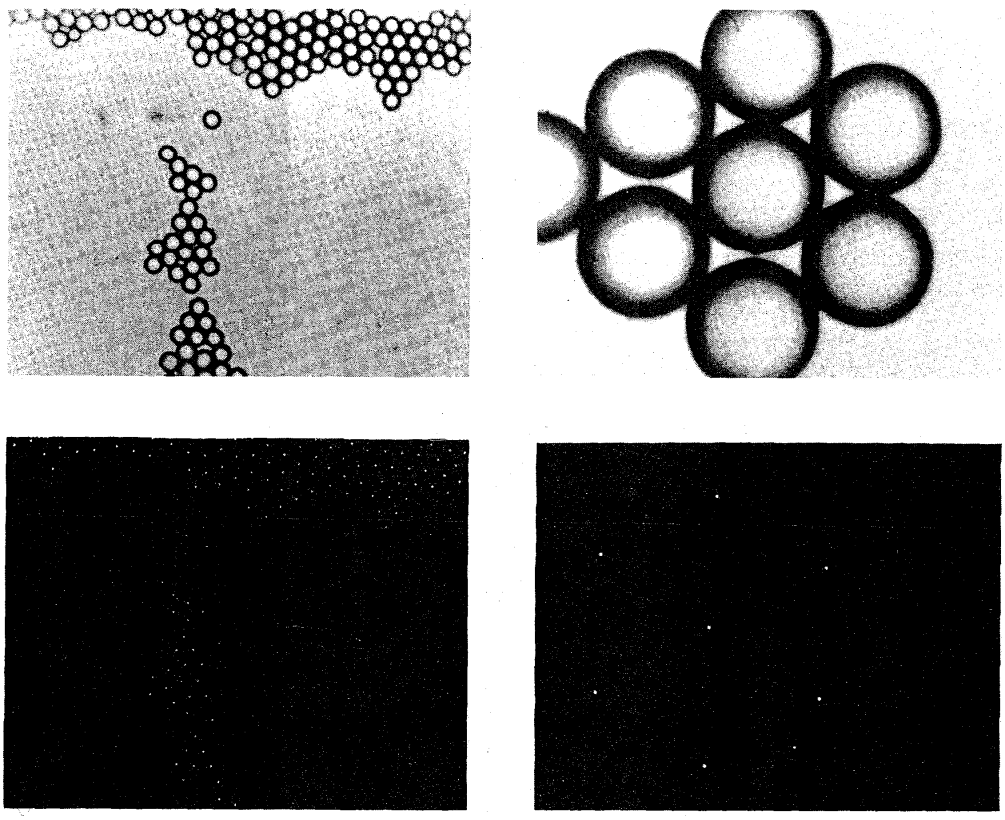

Figure 4. Focal spots of microspheres of 3- and 30-μm diameter.

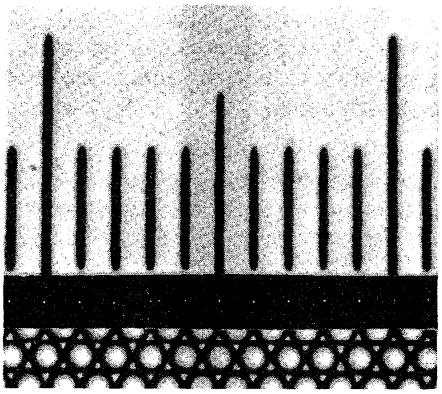

Figure 5. An object micrometer and a 10-μm microsphere scale.

3.1.1 Microsphere scales involving 1 to 100 spheres

In the following paragraphs the accuracy of a microsphere scale will be estimated for cases involving 1 to 100 spheres. The selected confidence level is 95% (2 sigma).

a) A single sphere

A single sphere selected at random will have a diameter D given by:

$$D = \bar{D} \pm 2\sigma_D = (9.89 \pm 0.04) \pm 2 \times 0.09\ \mu m$$

$$= 9.89 \pm 0.21\ \mu m.$$

Of the 0.04 μm uncertainty, 0.01 μm is a random part and 0.03 μm is a systematic part [5]. The random part adds in quadrature to the $2\sigma_D$ contribution which is random also, giving 0.21 μm total. Due to edge diffraction this distance will be read out with considerably larger uncertainty: about 0.5 - 1 μm.

b) A contacting sphere pair

When the spheres are illuminated with parallel light a focal spot forms above each sphere: the separation distance of the spots is equal to the sum of the radii of the two contacting spheres. When the sphere diameters have a normal diameter distribution, the sum of two radii will be normally distributed also, with a mean diameter of $\bar{D}$ and a standard deviation equal to $\sigma_D/\sqrt{2}$.

At the contact area the spheres will be slightly flattened due to mutual van der Waals attraction resisted by elastic deformation forces [5]. This causes a calculated 0.02 μm decrease in sphere center distance (see Sect. 3.4). The expected sphere center distance, C, as represented by the focal spot spacing, is:

$$C = \bar{C} \pm 2\sigma_D/\sqrt{2}, = (9.89 - 0.02 \pm 0.04) \pm 0.13\ \mu m$$

$$= 9.87 \pm 0.16\ \mu m.$$

Sphere pairs can be found in the unordered microsphere grouping on the microsphere slide. It would not be possible to read a single 10-μm division of a calibrated stage micrometer from photomicrographs at accuracies aproaching 0.16 μm.

c) An eleven-sphere row

When spheres are arranged in a hexagonal array, each sphere cannot simultaneously touch all six of its neighbors (see Sect. 4.2). There is a distribution of small gaps between spheres, scattered throughout the array. The average gap width is $(0.46 \pm 0.03)\sigma_D$ [1].

This phenomenon causes the distribution of sphere centers to deviate from Gaussian; it can be approximated by a normal distribution with a standard deviation $\sigma_C = 1.1\sigma_D$ instead of $\sigma_C = \sigma_D/\sqrt{2}$, giving $\sigma_C = 0.10$ μm.

In an array row, the average value $\bar{C}$ for a sphere center distance will be equal to $\bar{D} + 0.46\sigma_D - 0.02$ (due to two-sided sphere flattening at the contact area) + 0.03 (due to sphere swelling occurring during the array deposition process) = (9.89 ± 0.04) + 0.05 = 9.94 ± 0.04 μm.

An eleven-sphere row will have 10 center distances, and a total length C_{10} given (at the 95% (2-sigma) confidence level) by:

$$C_{10} = 10\bar{C} \pm 2\sigma_D\sqrt{10} = 99.4 \pm 0.4 \pm 0.6 = 99.4 \pm 0.9\ \mu m.$$

The microscope slide contains array rows with lengths typically 10 – 20 spheres. The calibration of an ocular micrometer (an eyepiece containing a reticle scale) can be done with an accuracy of about 0.7% when using the microsphere slide. However, if the purpose is to calibrate magnification in the film plane of a photographic microscope, then improved accuracies are possible, as shown below.

d) A microsphere row combination containing 100 center distances

Improved accuracy can be obtained by measuring several neighboring (parallel) rows to give a longer total length. If the microscope has been calibrated for radial image distortion, the measured row lengths can be corrected, and the film scale for zero distortion can then be obtained with considerable accuracy. Assuming one has measured 10 parallel rows of 10 center distances each, one finds the following:

$$C_{100} = 100\bar{C} \pm 2\sigma_D\sqrt{100} = 100(99.4 \pm 0.04) \pm 2.0 = 994 \pm 6\ \mu m.$$

It is therefore possible to determine the magnification in the film plane of a photographic microscope with an accuracy approaching 0.5%, provided all other variables are under control. The major variables are:

1) Image distortion

If no correction is to be made for image distortion only the central 20 - 25 % of the field of view diameter should be used. The FOV diameter will then be some 50 spheres or 0.50 mm. The corresponding image magnification will be fairly low, about 200× if 4 × 5 inch sheet film is used.

For higher magnification, for instance 800× to 1000×, the separately measured row lengths should be corrected for image distortion; a procedure is given in Section 3.2.

2) For maximum accuracy, a number of repeated film exposures should be used, in order to reduce the effect of fluctuations in magnification caused when inserting fresh films (see Sect. 3.3). A useful number is five repeated exposures.

3) As with all microsphere row length measurements, the rows should be visually flawless, without cracks or curved rows. Such flaws would

indicate the presence of slack in the array and therefore loss of contact between spheres which would introduce measurement errors.

3.1.2 Comparison with a stage micrometer

A microsphere scale consists of a row of small and equispaced circular spots. Their spacings can be read with high resolution, about 0.03 μm when using photomicrography and 10-μm spheres. However, because the sphere diameters are only statistically known and not all spheres actually touch each other, the accuracy of such a microsphere scale is limited, to about 1.0% for a single 100-μm length, and 0.6% when using 10 such lengths.

With a stage micrometer the situation is the reverse: its scale divisions can be calibrated with great accuracy (about 0.04 μm for a micrometer of lithographic quality using complex photo-electric instrumentation and an interferometric object stage). However, the resolution of the scale readout by means of photomicrography is considerably less: about 0.2 μm because of the relatively large widths of the lines that mark the scale divisions (2.5 – 3 μm, compared to 0.7 μm for focal spot diameters produced by 10-μm spheres and photographed at 500×) as indicated in Figure 5. As a result, the photographic accuracy of a calibrated stage micrometer is about 0.2 – 0.3% for a 100-μm length and about 0.5 – 1% for an uncalibrated one. If the length of a selected microsphere row is compared with a corresponding length segment of a calibrated stage micrometer, the possibility exists to obtain a microsphere "ruler" or scale with almost the same accuracy. This is because the losses in accuracy from image distortion corrections and from pinpointing the focal spots are relatively small.

Hexagonal microsphere arrays can be deposited on a microscope slide with ease; using a mean sphere size in the range from 1 - 30 μm the rows are typically 70 - 15 spheres long, respectively. A microsphere array can thus serve as a two-dimensional microsphere scale, with a selectable length of its divisions.

3.1.3 Readout of the photomicrographs

In many cases the image magnification in the photomicrograph will lie in the 100× – 1000× range. The focal spots that mark sphere centers and make up a microsphere ruler will then show up in the film as circular "dots", with diameters about 0.2 - 0.8 μm. The positions of their centers can be located with a precision of 0.01 - 0.03 μm, using a low-power microscope with crosshairs.

Adjacent dots representing touching microspheres will then be spaced 1–10 mm apart and the microsphere rows will have lengths ranging from about 10 mm to a full film frame (124 mm for 4×5 Polaroid[1] positive film).

The choice of which equipment to use to measure the films will depend on several factors such as cost, skills of the operator, availability of components or setups that can be converted to use for film readout, etc. Several possibilities are listed below.

---

[1] In order to adequately describe materials and experimental procedures, it was occasionally necessary to identify commercial products by manufacturer's name or label. In no instance does such identification imply endoresement by the National Institute of Standards and Technology not does it imply that the particular products or equipment is necessarily the best available for that purpose.

a) A coordinate measuring machine (CMM)

The mechanical probe of the CMM is replaced by a low-power microscope with crosshairs, the film is placed on the CMM table and held flat by placing a weighted sheet of glass or acrylic on it, and is illuminated obliquely from above the film with a microscope light (such as the Nicholas Illuminator from Bausch and Lomb).

The microscope is centered manually over each dot to be measured, the corresponding CMM coordinates are recorded, and the positions are then corrected for image distortion in the film (Sect. 3.2). This readout process may be automated, using a TV image sensor with centroid-seeking circuitry and a CMM with X-Y travel under computer control.

The positions of the dot centers in the film can be found visually with 0.015 – 0.02 mm precision using a low-power microscope with crosshairs. A TV-microscope can achieve better than 0.01-mm precision. The X-Y scales of a CMM have accuracies considerably better than 0.01 mm.

b) A toolmaker's microscope

These microscopes with crosshairs have a specimen stage with X-Y micrometer drives, typically 25 × 25 to 100 × 100 mm. The stage travel can be read with a precision of 1 - 2 μm, the scale accuracy being typically 1 - 5 μm.

c) A standard microscope with graduated specimen stage

These stages typically have a travel of 50 × 75 mm with millimeter scales that can be read to 0.05 – 0.1 mm. Their accuracy is typically 0.05 – 0.10 mm also.

d) A reticle magnifier

This is a low-power (7× to 10×) magnifier with a wide, flat field. It contains a reticle scale which is typically 20 mm long, with 0.1-mm divisions. The scale can be read out to 0.02 - 0.03 mm. Scale accuracy is typically 0.05 mm.

It is apparent that microsphere row lengths can be measured with equipment as simple as d). If individual microsphere center spacings are to be measured in order to determine diameter distributions, then a technique at least as precise and accurate as d) is required. A useful all-round approach is b). However, the CMM technique, a), is by comparison the best.

3.2 Image distortion and magnification in a microscope

The magnification of a microscope can be found by measuring the image length of a stage micrometer placed such that it crosses the center of the field of view. When this is used to determine the length of a microscopic object or feature, the object must be positioned such that the end points of the feature dimension coincide with the stage micrometer marks photographed earlier, in order to avoid errors due to image distortion.

If the object is considerably smaller than a field of view diameter, if it can occur anywhere in the field of view, and if an accurate measurement is sought, the "local" (off-

axis) value of the magnification can be used rather than its field-averaged value. This value can differ by several percent from the magnification found above, due to image distortion. This distortion can also cause the local magnification to be dependent on object orientation.

In the following paragraphs a method is described to find the image distortion and the image magnification as a function of off-axis distance. Accuracies of 0.5% are possible, permitting the photographic microscope to be used for high-precision two-dimensional micrometrology using low-cost standard equipment. In Section 3.2.1 the principle of this method is outlined, followed by a worked-out example in Section 3.2.2.

3.2.1 Principle

Image distortion causes imaged points of an object to be displaced from their expected positions in the image plane. For high-quality well-centered optics, these image point shifts are radial ones: an image point located at an expected off-axis distance r will have shifted radially to r+f(r), with f(r)<<r.

A radially oriented line image AB with length L will have its end points shifted by different amounts as indicated in Figure 6a, point A will move from r_1 to $r_1 + f(r_1)$ and B shifts from r_2 to $r_2 + f(r_2)$. Consequently, the length $AB = L = r_2 - r_1$ will change to:

$$AB = r_2 + f(r_2) - r_1 - f(r_1) = r_2 - r_1 + (r_2 - r_1)\left.\frac{df}{dr}\right|_{\bar{r}}$$

The local radial magnification M_r differs by a small fraction $\left.\frac{df}{dr}\right|_{\bar{r}}$ from its on-axis value M_o.

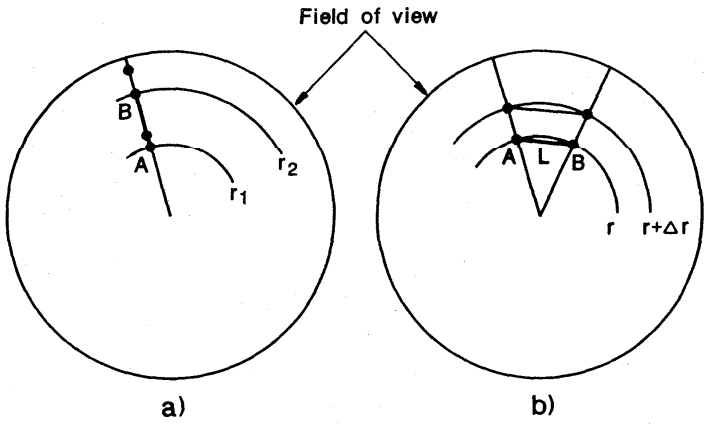

Figure 6. Calculating radial and tangential magnification
a) radial magnification b) tangential magnification

One can measure M_r as a function of r by making a series of photographs of a given length segment oriented radially in a series of positions spanning a field-of-view diameter, and measuring the changes in the imaged length. Expressed in terms of its on-axis value, these length changes are equal to $\frac{df}{dr}$ from which f(r) can be found by graphic integration. A faster way requiring only one additional photograph is to utilize a whole row of equal-size length segments, shifting it in-line by one (or a few) segment lengths, and measuring

how much each segment changed in length as a function of: initial off-axis distance, length of the shift, and length of the line segment. The row of equal-size line segments is conveniently represented by a row of equispaced focal spots as part of a hexagonal microsphere array. The changes in length of each segment in the row are found as follows:

the line segment, with its end points initially located at $r_1 + f(r_1)$ and $r_2 + f(r_2)$, is shifted by an amount Δr causing the end points to move to new positions $r_1 + \Delta r + f(r_1 + \Delta r)$ and $r_2 + \Delta r + f(r_2 + \Delta r)$. The new segment length is :

$$r_2 + f(r_2 + \Delta r) - r_1 - f(r_1 + \Delta r)$$

$$= r_2 - r_1 + f(r_2) + \Delta r \left.\frac{df}{dr}\right|_{r_2} - f(r_1) - \Delta r \left.\frac{df}{dr}\right|_{r_1}$$

$$= L\left(1 + \left.\frac{df}{dr}\right|_{\bar{r}}\right) + \Delta r \left.\frac{df}{dr}\right|_{r_2} - \Delta r \left.\frac{df}{dr}\right|_{r_1}$$

$$= L\left(1 + \left.\frac{df}{dr}\right|_{\bar{r}}\right) + L \left.\frac{d^2f}{dr^2}\right|_{\bar{r}} .$$

The radial shift Δr of each length L has caused length changes proportional to $\frac{d^2f}{dr^2}$, and a graphic integration will yield the radial magnification $M_r = M_o\left(1 + \left.\frac{df}{dr}\right|_{\bar{r}}\right)$.

Different results are obtained if the line segment AB is oriented tangentially, as in Figure 6b. Image distortion f(r) causes the associated arc length ar to change to $\alpha r + \alpha f(r) = \alpha r\left(1 + \frac{f(r)}{r}\right)$. The chord length AB changes in proportion, and the tangential magnification M_t changes to $M_t = M_o\left(1 + \left.\frac{df}{dr}\right|_{\bar{r}}\right)$. If the image distortion happens to be proportional to r, $f(r) = ar$, then M_r and M_t will be equal: $M_r = M_t = M_o(1 + a)$.

M_o itself can be found by imaging a known object length and correcting the measured image length for the effects of image distortion. The ratio, reflecting the absence of image distortion, is the on-axis magnification value M_o.

3.2.2 An example

A row of 10-μm microspheres was shifted in-line by 30 μm, and the changes in focal spot center distances along the row were measured (see Fig. 7a). The magnification could be obtained from that Figure by fitting a curve plus a graphic integration. Instead, the curve fitting and integration (with its errors) was replaced by a cumulative summation process described below, using the data points of Figure 7a. This resulted in Figure 7b in which the data scatter now showed up as well. A curve was fitted showing M vs. r, and a graphic integration yielded f(r) (see Fig. 7c).

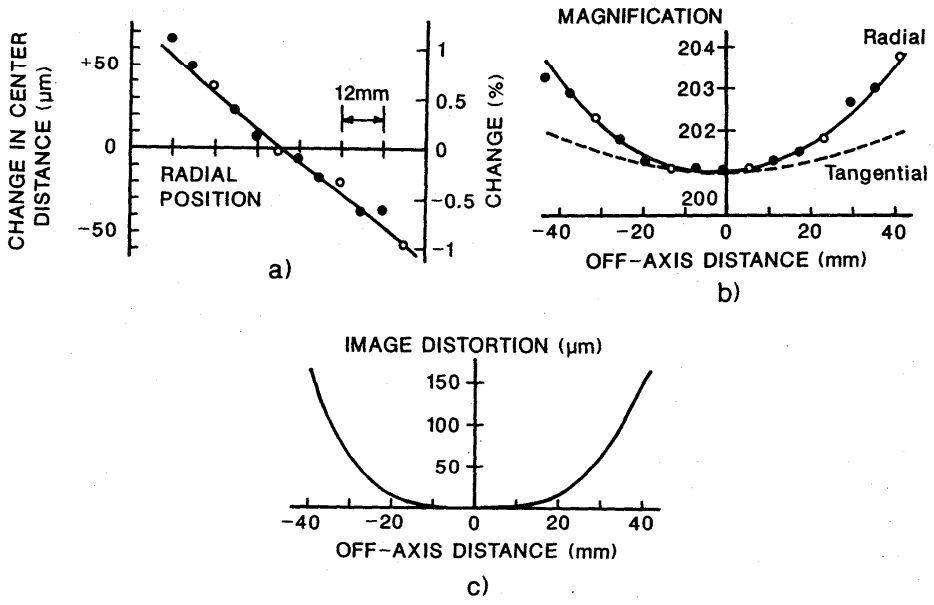

Figure 7. Finding image magnification and distortion.

The row was shifted by an amount 3D rather than D in order to improve data resolution in Figure 7b. It did not result in an averaging of the obtained radial function over 3D but only over D, as will be apparent from the following description of this cumulative summation process to obtain Figure 7b from Figure 7a.

Starting at the first (left) position, the accumulated length changes are found when a focal spot center distance of length D is shifted in-line by 3D; the data points obtained are marked as small circles in Figure 7b. The process is repeated starting at the second position, then again at the third. The result is three data sets which are arranged such that they fall on a common curve, M_r vs. r. From this the image distortion f(r) vs. r is found (Fig. 7c). Also marked in that Figure is the calculated tangential image magnification M_t.

The microscope optics consisted of a 20×/0.50NA objective, a 2× relay lens, and a 12.5× photo eyepiece, giving a photographic magnification of nominally 500× and a 200-μm field of view.

The accuracy of the magnification data shown in Figure 7b can be estimated as follows. A 100-μm section of a stage micrometer was used; its calibration, done at NIST, had an accuracy of 0.04 μm. The photomicrographs were read out with a precision of 0.1 μm. The image distortion increased the apparent length of the 95-μm object by 0.7 μm, with 0.07-μm uncertainty. This value was arrived at in an interative process, because the data in Figure 7c are derived straight from Figure 7b while the data in Figure 7b depend – albeit weakly – on those in Figure 7c. In addition, errors are introduced by spurious changes in magnification caused when placing new sheet film in the cassette (see Sect. 3.3). These changes can amount to 0.2% when using a single photograph, or 0.1% when five repeated photographs are used. The above considerations, and similar ones for the off-axis variations in magnification lead to estimates for the accuracy of the magnifications M_o, M_r and M_t amounting to 0.3 - 0.4%.

When a photomicrograph containing dimensional information is measured under computer control, the image distortion curve and the value for M_o are used to construct an X-Y reference frame in the object plane in which the object is then mapped. If, however, the object is relatively small and manual readout is used, a measuring microscope or a reticle magnifier may be used and the data are then evaluated based on local magnification values. If the object contains very sharply defined surface features allowing high-resolution micrometrology, then the question of tangential vs. radial magnification may also come in.

3.3 Spurious changes in microscope image magnification

When a microscope is refocused its object distance changes. Its image distance measured from the last imaging lens (which can be the photo ocular or equivalent) changes and the image magnification changes in proportion. If the film plane is held stationary the image scale in that plane stays almost constant, although the image at the film plane will lose sharpness. If on the other hand a film sheet is replaced and the new film is now at a slightly different position on the optical axis, the film scale will vary. The film-to-eyepiece distance is typically 150 – 200 mm and the position tolerance of typical Polaroid sheet film in its cassette is about 0.1 – 0.2 mm, therefore spurious magnification changes can be expected at the 0.1 percent level.

This effect can be measured as follows. A row of microspheres is placed so as to cross the center of the field of view, the sphere preparation is illuminated with parallel light and the resultant row of focal spots is photographed several times (for instance five times). Center distances between focal spots (ranging from D, 3D, 5D,... to a full field diameter) are measured in each photograph, and the scatter in each measured distance is calculated. A graph is made of this scatter as a function of the measured distance, resulting in a plot as in Figure 8. For large distances the plot approaches a straight line going through the origin. The slope of this line represents that part of the scatter which is proportional to length, and thus is caused by fluctuations in magnification (0.2% in the Fig.).

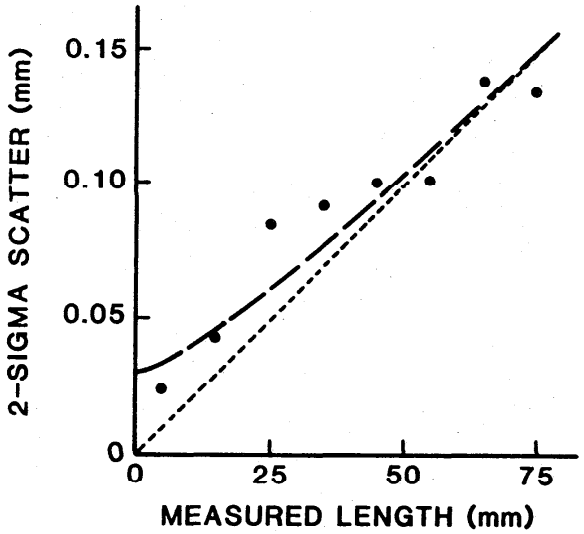

Figure 8. Scatter in length measurements vs. measured length.

Such an uncertainty in magnification applies to every photograph taken with the microscope. It is caused by the use of flexible film sheets and a film cassette without a vacuum platen.

Because the film is held by its edges, these magnification fluctuations will be maximum near the center and essentially constant only over a relatively small central area (one-half of the field of view or less), therefore the sphere rows used should not be too long.

3.4 Use as a standard for particle sizing instruments

Single spheres, with statistically known diameters, can be used as test objects for particle sizing instruments that analyze particle images. If an odd number of particles (for instance three) touch each other to form a closed loop, measurements of all center distances will then yield all diameters (after correction for sphere flattening, see below), thus providing accurately known test objects.

When two spheres touch, van der Waals attraction forces [4] at the initial contact area will also pull adjacent areas into contact, much like two optical flats exhibit progressive contacting when initially pressed together at one area. This phenomenon is resisted by elastic sphere deformation, resulting in a flattening of the spheres at contact and in a decrease of the center distance between touching spheres. As already mentioned in section 3.1.1, this decrease amounts to a calculated 0.02 μm.

The calculation is based on a paper by Muller et. al. [6], who have analyzed the balance between sphere-to-sphere attraction and sphere deformation. They give expressions for the flattening of spheres in contact with a flat substrate. These estimate the sphere deformation at and around the contact area, and indicate that the active non-contacting zone is relatively small (when no external forces are present). In that case the flattening of a sphere contacting an equal-size sphere will be essentially equal to that of a sphere contacting a plane. One can then double the Muller expression to find the decrease in sphere center distance C due to van der Waals attraction. This decrease ΔC is equal to:

$$\Delta C = \frac{1}{4}\left(\frac{3(1-\eta^2)^2 R A^2}{2E^2\varepsilon^4}\right)^{1/3}, \text{ where}$$

η = Poisson constant (= 0.3 for polystyrene)

R = sphere radius (= 5×10^{-4} cm)

A = Hamaker constant (= 1×10^{-12} erg for polystyrene)

E = Young's modulus (= 3×10^{10} dn/cm^2 for polystyrene)

ε = distance of closest approach (= 3×10^{-8} cm).

This gives $\Delta C = 2\times10^{-6}$ cm = 0.02 μm.

4. THE MICROSPHERE SLIDE USED IN EDUCATION AND TRAINING

In the following paragraphs a number of subjects are discussed that can form a basis for a test or measurement in the Physics Laboratory, or a classroom demonstration. The student will gain experience in – and an appreciation for – aspects of micrometrology. A close inspection of the microsphere slide will also reveal items that are out of order, and which can make the life of a particle analyst miserable: spheres that are "clearly" larger or smaller than the main population and thus must be considered outliers, dust and dirt which was impossible to filter out or to otherwise remove prior to sealing the slide, polystyrene particles of strange shapes (twin spheres, or elongated spheres), sealed-in "crystals" that defy identification, and so on.

This chapter is primarily addressed to you, the student, and we hope that you will get inspiration and fun out of your measurements done on the slide.

4.1 Array Sizing

This is a technique to measure the mean size of a collection of microspheres which have essentially the same diameter (the spheres are "monosize"). The spheres are deposited

in hexagonal arrays containing many straight rows, and measurements of row lengths containing a known number of microspheres yield a surprisingly accurate value for the average diameter of the spheres [2,3].

The row lengths can be measured in several ways. You can use the aerial image itself, in which case the measurements are made by an eyepiece micrometer, or you can use photomicrographs. The settings can be made on the apparent center of the spheres, or on the contact areas (see Fig. 9). In both cases, use is made of the sensitivity of the human eye for symmetry: the eyepiece crosshairs can be set with a resolution of less than one-tenth of the sphere diameter, or better than 1 micrometer.

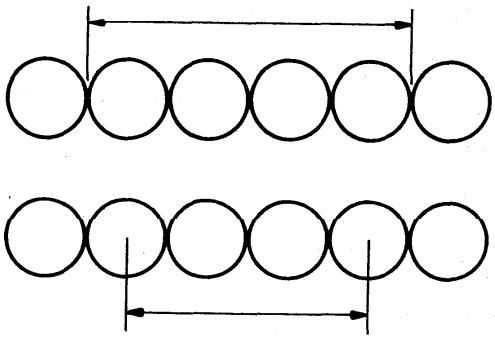

Figure 9. Microsphere settings in array sizing.

A different way is to not use microsphere images at all. Instead, one illuminates the spheres with parallel light, approximated by stopping the condensor way down or by taking it out altogether. The spheres refract this light into very small focal spots (see Sect. 3.1), the microscope is refocused on the common back focal plane containing these spots (which mark the sphere centers in the field of view), and the row lengths are measured as the distance from the center of the first spot to the center of the last spot. In this way the length measurement can be done with improved resolution: less than 0.05 micrometers when using photomicrographs (see Fig. 1b).

For these measurements the microscope magnification and image distortion should be well-known; a calibration procedure is given in Section 3.2. Error sources will be the Kubitschek Effect (Sect. 4.2), sphere flattening (Sect. 3.4), and possibly sphere swelling (Sect. 5.2).

4.2 The Kubitschek Effect

Kubitschek [1,5] has pointed out that a two-dimensional hexagonal array structure of microspheres having a distribution of sizes will contain a distribution of air gaps throughout the array; the average air gap width between spheres is $0.46\sigma_D$. As a result, the mean diameter (D) is found oversize by that amount. Consider for instances a smaller sphere surrounded by six equal-size larger ones. The smaller sphere can touch only two of the six, leaving four air gaps in that part of the array.

The existence and magnitude of the Kubitschek effect can be found by making mean diameter measurements using two types of close-packed microsphere structures made from the same microsphere material: one which has the air gaps (hexagonal arrays) and the other which does not. Examples of the latter structure are square and rhombic arrays, and strings of spheres in contact (Figs. 1 and 10). In square and rhombic array structures each sphere can in principle touch all of its four neighbors. In string structures the attention will be focused on those spheres that have no more than two neighbors: air gaps need not form during formation of such string structures.

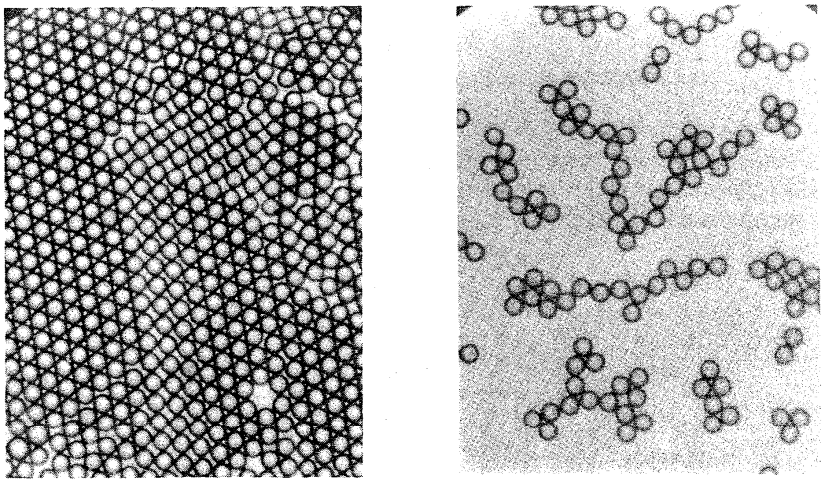

Figure 10. Microsphere structures without air gaps.
a) Rhombic arrays b) String structures

Square or rhombic arrays form rarely; your slide may not have any. However, the microsphere slide contains beside an area of hexagonal arrays also an area of unordered string-like close-packed microsphere structures. By determining a large number of sphere-to-sphere distances from measurement of center distances of these structures viewed in parallel light) you will obtain a mean value of the sum of sphere-pair radii. This value is equal to the mean diameter of the microspheres themselves (Why?).

A comparison between the mean diameter values found from arrays (D) and from strings ($\bar{D}_o$) will show them to be significantly different, with the array value being larger. The predicted value of that difference is $\bar{D} - \bar{D}_o = 0.46\sigma_D$ [1]; this can be confirmed experimentally by measuring also the size distribution of the microspheres on the slide (see Sect. 4.3). The material on the Microsphere Slide has a normal size distribution with $\sigma_D = 0.09 \pm 0.01$ μm. If the comparison between $\bar{D}$ and $\bar{D}_o$ is to be done at a level of 0.01 μm with 2-sigma (95%) confidence, how large should the number of measured spheres be?

4.3 Measuring the microsphere diameter distribution

For this measurement the unordered sphere structures are used. The structures are illuminated with parallel light, and photomicrographs of the focal spot patterns are made. A large number (300 – 1000) of center distances between adjacent spots in the film are measured carefully, then converted into distances (μm) in the object plane. For this conversion the microscope magnification as a function of off-axis distances should be known (see Sect. 3.2).

To avoid possible errors introduced by "invisible" (<0.2 μm) air gaps, the measurement path is selected such that the measured sphere grouping is not overconstrained. During the drying process each sphere would then have been able to freely come into contact with its neighbors. This implies in general a measurement path in which each measured sphere has no more that two neighbors. Also, each sphere must be measured only once (Why?).

The center distance (C) distribution is plotted and examined. If it is found to be a normal one (How?) then the diameter (D) distribution is normal also, with a mean $\bar{D}$ equal to $\bar{C}$ and a standard deviation $\sigma_D = \sigma_C\sqrt{2}$ (Why?). The mean diameter and the diameter distribution of the microsphere material on the microsphere slide was measured in this way at NIST; the result is shown in Figure 11. This microsphere sizing technique by optical microscopy is called "Center Distance Finding" (CDF); it is described in detail in Reference 5.

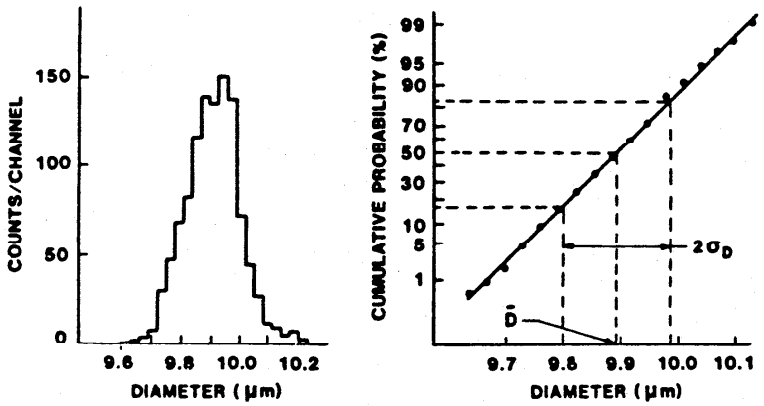

Figure 11. Diameter distribution of Microsphere Slide material.

The entire width of the diameter distribution of the Microsphere Slide material is only one-half of a micrometer. To map out such a size distribution, diameter measurements are needed with a resolution of better than 0.1 μm. This is quite feasible with electron microscopy but not when optical microscope images are used. Yet the same optical microscope can make diameter measurements by CDF with a resolution better than 0.05 μm. Why does that technique work so well? The reason is that we do not use the image resolution capabilities of the microscope, instead we use its position resolution for point images. The former represents the radius of an Airy diffraction disk (0.5 μm), while the latter indicates the resolution with which the center position of such a disk can be found (0.01 - 0.02 μm).

4.4 Do "contacting" spheres actually touch?

When microspheres are sized by Center Distance Finding it is necessary that the measured spheres be in contact with each other. How can we be confident that they are actually in contact? Inspection of the optical images in string structures will not tell us; air gaps smaller than about 0.2 μm go unnoticed. There is an indirect test however, which goes as follows. Look for a microsphere structure that contains two or more triangular arrangements, as in Figure 12. Starting with one triangle, a measurement of its three center distances leads to the three diameter values. The diameter of spheres farther away are found from center distance measurements between a sphere of known diameter and the adjacent unknown sphere. If this is done for a string of spheres starting from two different triangular structures, one obtains two sets of diameters. If these are equal within experimental limits, then this can be considered an indication that air gaps are absent. If unequal data sets are caused by one air gap, one can tell where that gap is and how wide it is (How?).

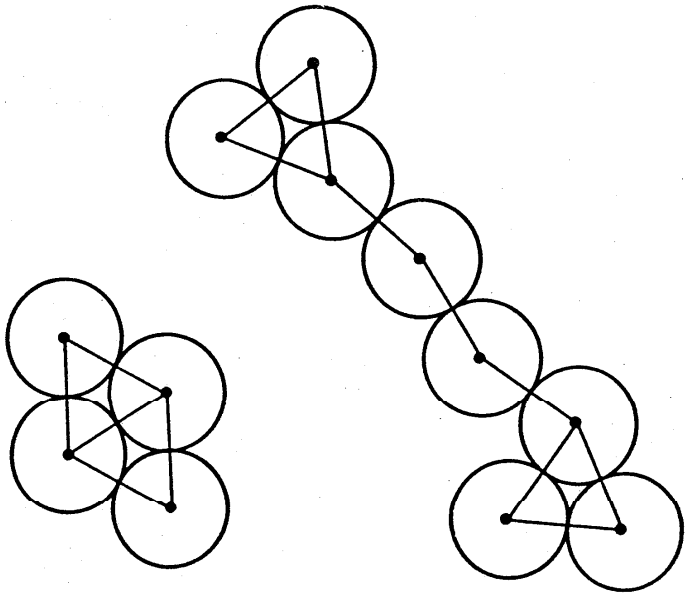

Figure 12. Detecting air gaps by measuring selected microsphere structures (see text).

An argument that air gaps should exist in close-packed hexagonal microsphere structures was discussed in Section 4.2 (the Kubitschek Effect). A confirmation of this can be found when center distance distributions are measured in hexagonal and in unordered structures; distributions as in Figure 13 are then found. The random structures produce a Gaussian distribution, as expected. Measurements on the array structure appear to indicate greater numbers of larger spheres; this is consistent with the notion that spheres and gaps are measured together. The distorted distribution cannot be caused by sphere deformation, because such spheres would have to be out of round by several percent (Why?) and their focal spots would then be elliptical by some 20 – 40 percent, which would be easily detected (see Sect. 4.5). Such deformed spheres are not present in any large amounts on your slide. It can thus be concluded that the skewed distribution in Figure 13 is due to a distribution of air gaps in the array. These gaps are on the average only some 0.05 – 0.10 μm wide.

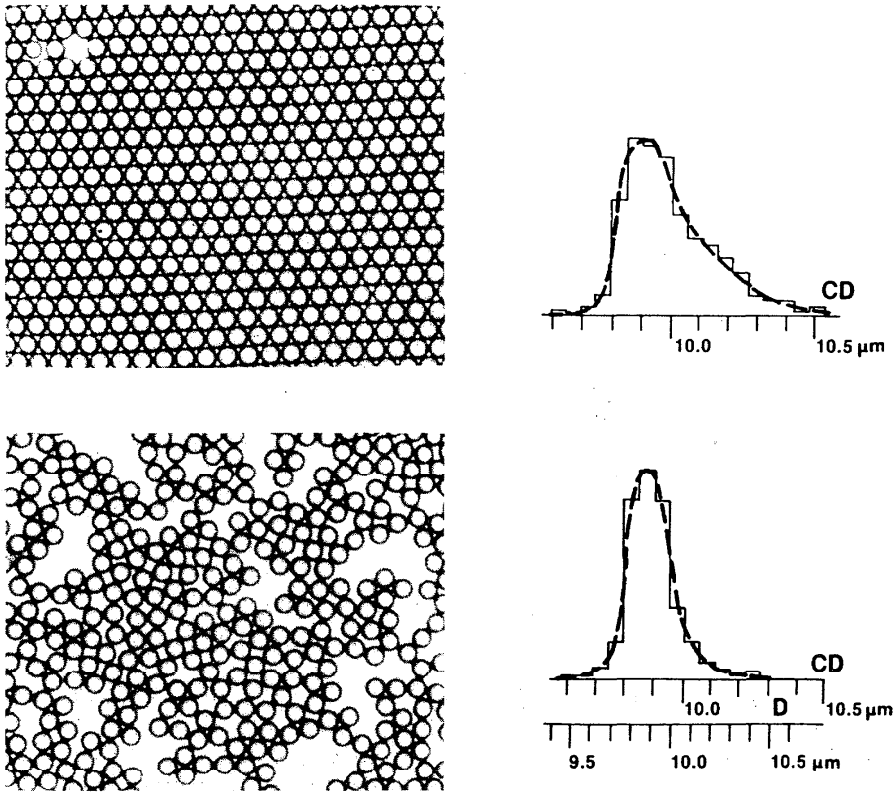

Figure 13. Air gaps in hexagonal arrays distorting center distance measurements.

4.5 Measuring sphere roundness

Figure 14 shows that microspheres with distorted shapes cause focal spot distortion. When the sphere is slightly oval-shaped, the centers of the two osculating spheres will be separated by a small amount and the focal spot will be elongated by the same amount (Why?). This is illustrated in Figure 15 for 10-µm spheres. The distorted spot with size 0.7 µm is elongated some 10%, corresponding to a calculated non-sphericity of 0.07 µm, or 0.7% of the sphere diameter. Such information could not be found from the microsphere images themselves. Your microsphere slide likely will have some distorted spheres.

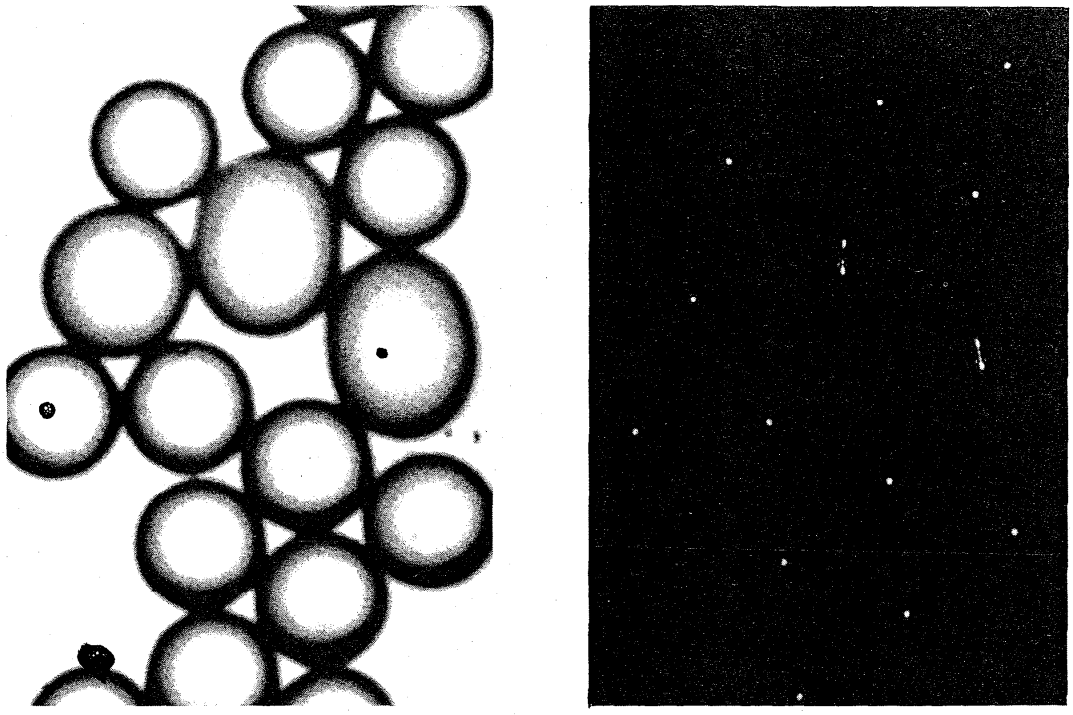

Figure 14. Focal spot shape affected by microsphere deformation:
a) deformed 30-μm spheres b) deformed focal spots

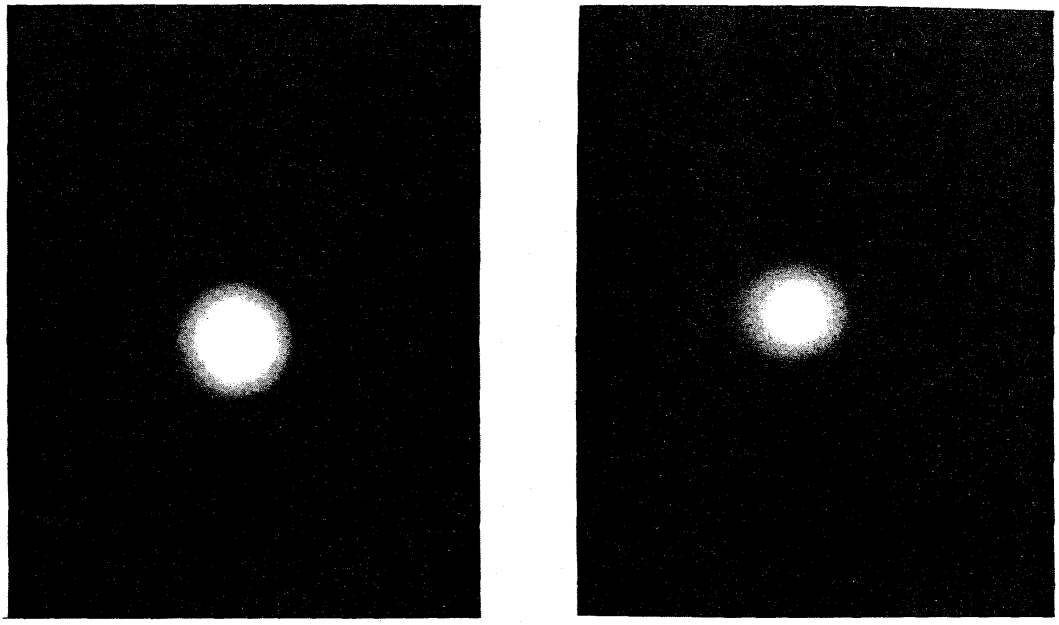

Figure 15. Normal and elongated 0.7-μm focal spots of 10-μm spheres.

4.6 Presence of dried solute matter between spheres

It is possible that your microsphere slide contains spheres that appear to be of two types, denoted as I and II, shown in Figure 16. Their focal spots form in two different planes that are some 5 μm apart, the grayish-looking type-II spheres in Figure 16 having the larger focal length. This can be explained by assuming that dried and transparent solute material was present around the contact area with the substrate surface; it makes such a sphere effectively a plano-convex lens instead of a spherical one. The solute material may, for example, be a surfactant used in making the arrays, (see Sect. 5). It causes the dark edge around the type-II sphere to be thinner than normal (Why?). You could argue that if much solute material dried up around the type-II spheres, there would likely be also solute material between them. The distances between sphere centers will then be larger than usual. What do you find for the average center distance in that case? What does that tell you about contacting spheres with dried solute material at their surface?

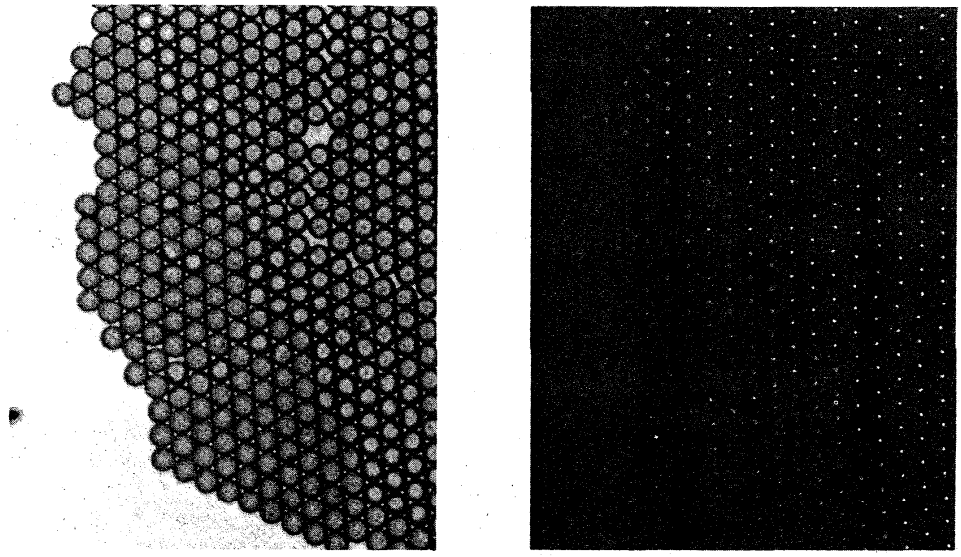

Figure 16. 10-μm spheres with focal spots in two different planes.

4.7 Simulation of Bragg diffraction

The ordered part of the Microsphere Slide contains many smaller areas that exhibit a single hexagonal ordering, like atomic particles in a microcrystal. The ordered areas have rows typically 5 – 10 spheres long. When such an area is illuminated with monochromatic parallel light from a laser, for instance with normal incidence as shown in Figure 17, light will emerge from the microsphere plane in discrete directions. This effect is caused by interference between cones of light emerging from each focal spot after refraction by the spheres. There is constructive interference in certain directions which are related to the microsphere diameter and the laser wave length (What is this relation?). This gives us an independent method for finding the microsphere diameter, by measuring the light patterns in two planes perpendicular to the optical axis. Examples are shown in Figure 18 b and c, using plane I for the microsphere images and plane II for viewing the interference patterns through the microscope. The refracted light can also be recorded without using a microscope, simply by placing a film at plane III.

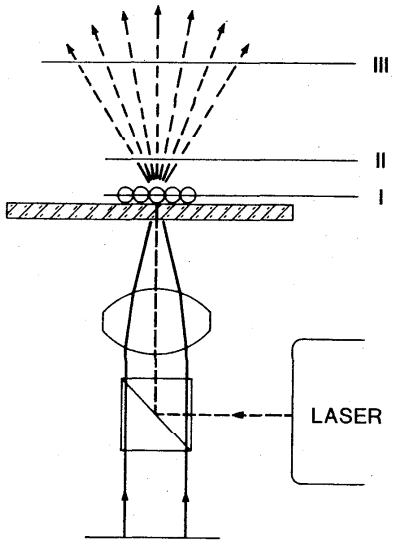

Figure 17. Microsphere illumination
used to produce Bragg-like patterns.

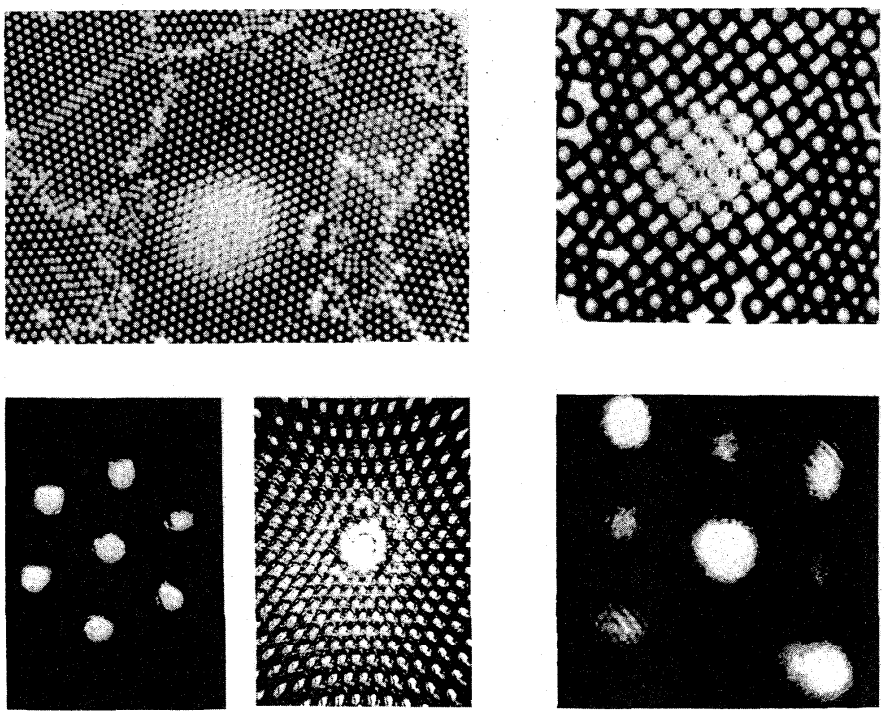

Figure 18. Bragg-like patterns caused by
a) hexagonal and b) rhombic ordering

Although the light patterns resemble Bragg x-ray diffraction patterns from microcrystals they are actually different, because we do not have three-dimensional structures of radiation-scattering point sources.

4.8 Lattice faults

The hexagonally ordered microsphere area shows features that are the two-dimensional analogs of three-dimensional lattice faults. Examples are shown in Figure 19. Their presence can be seen from microsphere imagery, and can be inferred from the Bragg-like patterns. Look for vacancies, slide planes, inclusions, microcrystallite boundaries, curved "lattice planes", and various types of ordering (hexagonal, square, rhombic). Even a single outsize particle can do considerable damage to a crystal structure, as illustrated in the Figure 20.

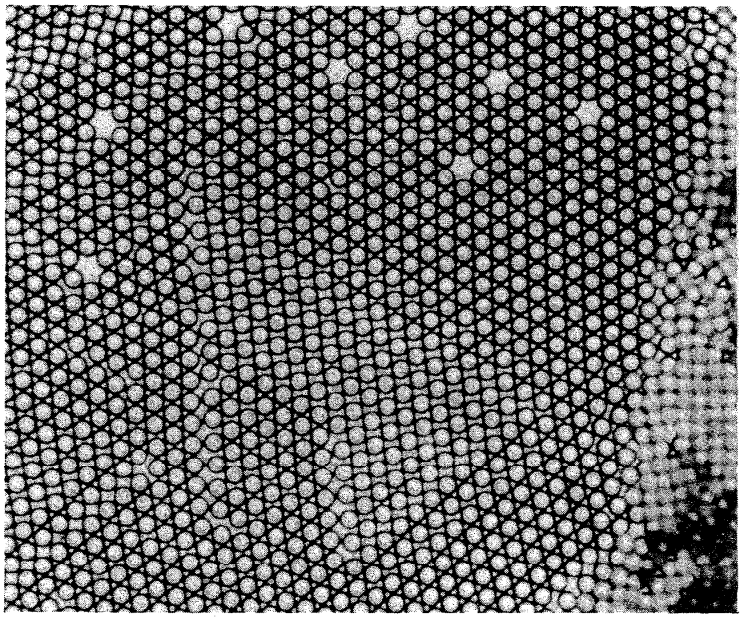

Figure 19. Microsphere arrays with various "lattice faults".

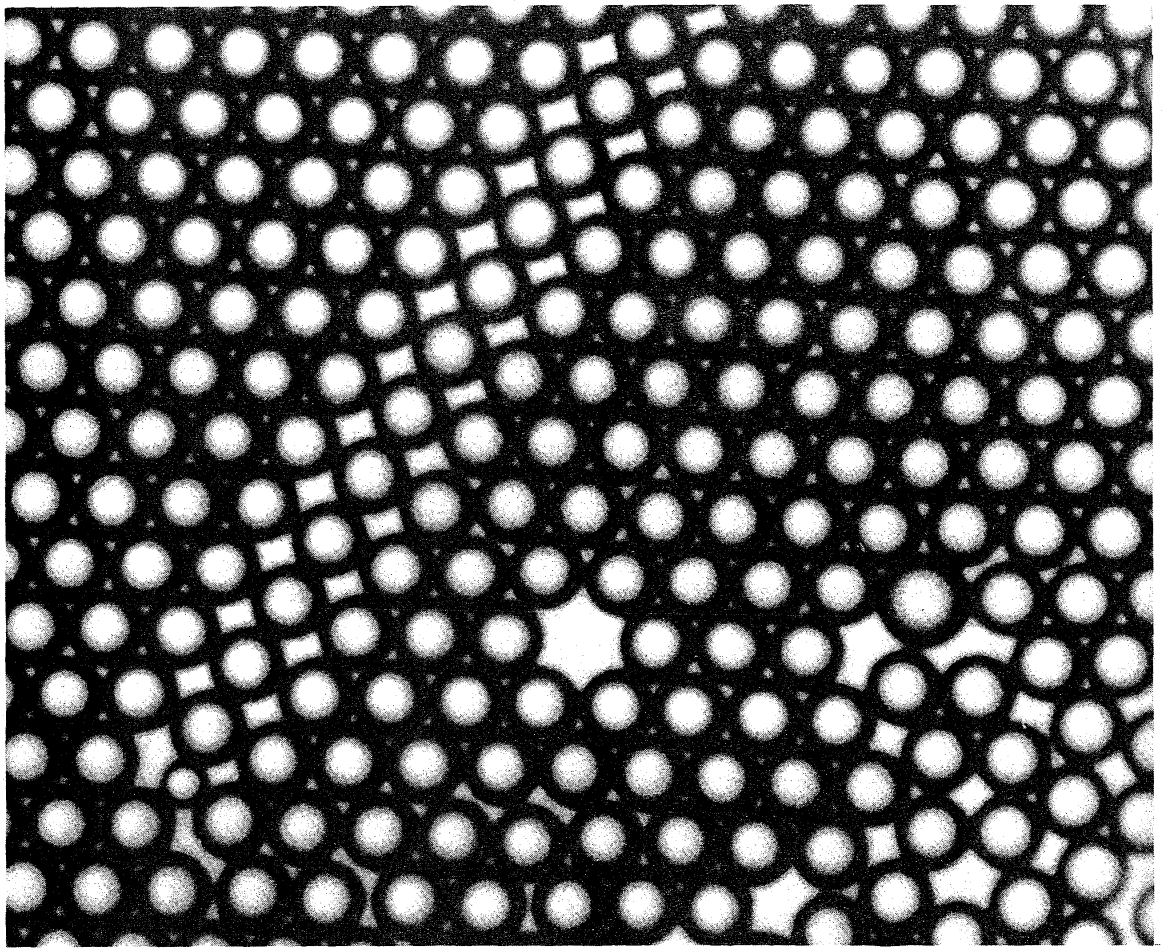

Figure 20. Crystal damage caused by a single outsize sphere.

4.9 Aspects of sphere position readout

Most high-power microscope objectives are corrected for one of two working conditions: 1) the space between the front lens and the object is filled with air only ("dry objective") or 2) the space is filled with material that has the same refractive index as glass (immersion oil, cover slip, any cement that the object is embedded in). The present situation is between these two extremes: two air spaces plus one layer of cover glass are present. For low-power objectives (20×, NA 0.5 or less) this hardly makes any difference, but objectives with larger NA may show some loss in contrast resulting in somewhat larger – but unshifted – focal spots. This loss in sharpness can be offset in part by the use of higher-contrast photographic film.

Establishing the center position of a photographed spot is facilitated considerably by a slight defocusing of the microscope away from the film plane. This causes the visual graininess of the film to be reduced, but does not introduce systematic errors (Why?).

5. MAKING THE MICROSPHERE SLIDE

5.1 Growing monosize polystyrene microspheres.

The microspheres were grown by a chemical process known as emulsion polymerization. This process is described in detail in References [7] and [8]; a brief sketch is given below.

A concentrated solution in water is prepared of a "surfactant", a material consisting of a compact, negatively charged, hydrophilic group of atoms (the "head") and a long hydrocarbon chain (the "tail") with a positive charge. Above a certain concentration value of surfactant in water, the surfactant molecules will arrange themselves into spherical assemblies with the "tails" inside and the "heads" outside, with each assembly containing essentially the same number of surfactant molecules. These fluid assemblies, called micelles, are much like small and monosize spheres (Fig. 21a).

To the micelle solution are then added measured amounts of two other chemicals: "initiator" and "styrene monomer". The initiator molecule looks like this:

$$RN{=}NR$$

with R being a hydrocarbon group.

The styrene molecule is shown below:

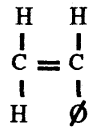

with Ø being a C_6H_5 group.

The two compounds diffuse into the micelles and cause them to swell, see Figure 21b. Then a polymerization takes place, which goes as follows. The initiator molecule splits in two parts, and each part (shaded in Fig. 21c) links up one after another with a number of styrene molecules, thus forming a chain. When two such chains combine the polymerization will stop. Using careful control of temperature, pressure, and time, the swollen micelles (which are no longer fluid) will contain a ball-shaped conglomeration of polymer molecules, each micelle containing equal amounts of material. When the surfactant is removed, we now have a collection of solid, monosize polystyrene microspheres (Fig. 21d).

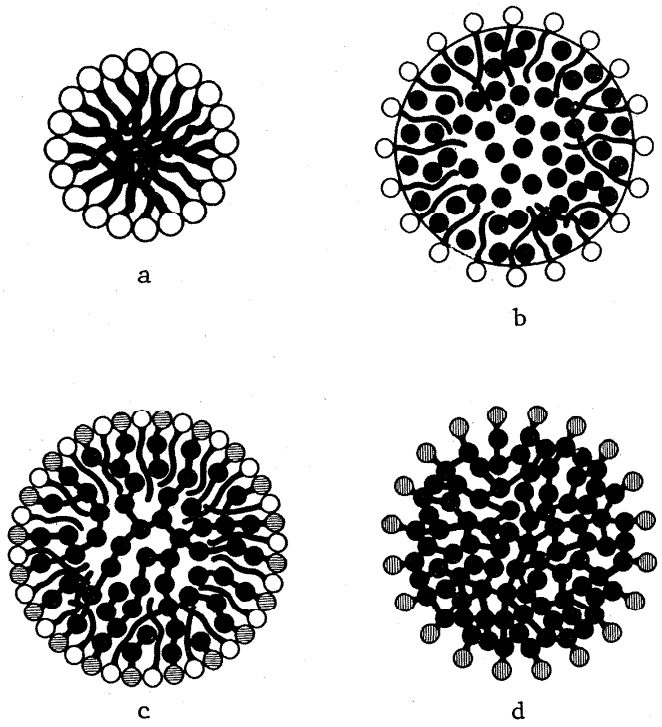

Figure 21. Microsphere formation by emulsion polymerization (courtesy L.B. Bangs, Ref. 8).

The chemical reactions describing the polymerization are as follows:

$$RN{=}NR \longrightarrow N_2 + 2R\bullet ,$$

$$R\bullet + \begin{matrix} H & H \\ | & | \\ C{=}C \\ | & | \\ H & \phi \end{matrix} \longrightarrow R{-}\begin{matrix} H & H \\ | & | \\ C{=}C\bullet \\ | & | \\ H & \phi \end{matrix}$$

where • denotes a free bond. After m more steps we have:

$$m\left[\begin{matrix} H & H \\ | & | \\ C{=}C \\ | & | \\ H & \phi \end{matrix}\right] + R{-}\begin{matrix} H & H \\ | & | \\ C{=}C\bullet \\ | & | \\ H & \phi \end{matrix} \longrightarrow R{-}\begin{matrix} H & H \\ | & | \\ C{=}C \\ | & | \\ H & \phi \end{matrix}{-}\left[\begin{matrix} H & H \\ | & | \\ C{=}C \\ | & | \\ H & \phi \end{matrix}\right]_m\bullet$$

This m-chain can combine with another chain to form a final product:

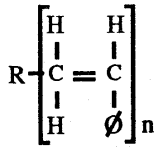

a polystyrene molecule. There are many such molecules in each micelle.

It is possible to repeat this process and make the monosize polystyrene microspheres larger [7,8].

5.2 Making preparations of contacting microspheres

A cover glass with a central hole is cemented to a microscope slide, the spheres are then deposited inside the circular area and a regular cover slide is cemented on top to seal off and protect the microsphere structures.

The microsphere structures feature contacting arrangements of two different types. Close-packing is obtained by letting a drop of microsphere suspension evaporate on the microscope slide. The surface tension forces of the evaporating liquid cause the drop to shrink until it dries, meanwhile pulling the spheres together, "raking them in" as it were.

In order to make the two types of close-packed structures: hexagonally ordered arrays and string-like unordered formations, two different suspensions in water of the same microsphere material are used, and deposited separately. One is the original Standard Reference Material (SRM 1960), with a sphere concentration of about 0.5% by mass, and containing about 0.005% sodium azide which inhibits the growth of organisms in the SRM vial; this is used to make the unordered strings. The other is a suspension containing 3% SRM spheres and 0.2% of a surfactant. This is used to make the arrays.

The purpose of the surfactant is to act as a lubricant between spheres as they are being pulled inwards when the liquid dries. The spheres which move as swarms, begin to order themselves when the thickness of the liquid is down to a sphere diameter or less. This ordering is "frozen-in" when the drying is complete, resulting in hexagonal arrays. In the other suspension, the absence of surfactant plus the much smaller sphere concentration causes the evaporating drop of suspension to break up during drying. This results in many small and unordered string-like structures of touching microspheres.

The surfactant was selected from the Triton-X series by Rohm and Haas. The compounds X-200 and up did not lubricate very well, causing shorter and less uniform arrays. X-100 worked well, but its smaller molecule is known to diffuse into polystyrene, causing it to swell slightly. The swelling of the 10-μm polystyrene spheres due to use of X-100 was measured and found to be only 0.03 μm; it was therefore used to make the microsphere suspension from which the hexagonal arrays were made.

The optical cement used for the three-piece glass assembly should not release any styrene monomer during curing, since this could diffuse into the polystyrene spheres and cause them to swell considerably. An example of this is shown in Figure 22. Note that the swelling did not cause the spheres to break loose from the substrate.

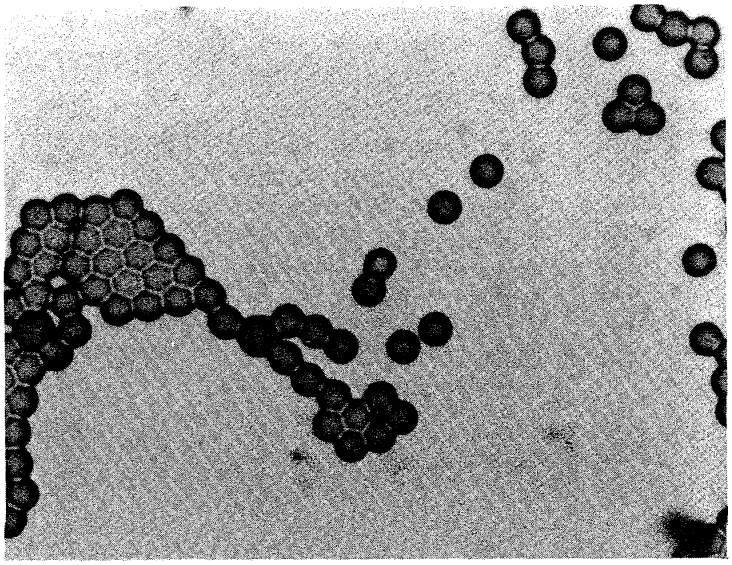

Figure 22. Swollen microspheres.

List of References

[1] Kubitschek, H. E., *Nature*, **192** (1961) 48.
[2] Robillard, F., and Patitsas, A. J., *Can. J. Phys.* **51** (1973) 2395.
[3] Hartman, A. W., *Powder Technol.* **39** (1984) 49.
[4] Bowling, R. A., *Solid State Science and Technology*, Sep. (1985) 2208.
[5] Hartman, A. W., *Powder Technol.* **46** (1986) 109.
[6] Muller, V. M., et. al., *J. Coll. Interf. Sci.* **77** (1980) 91.
[7] Kornfeld, D. M., NASA TM-86487, January 1985.
[8] Bangs, L. B., Uniform Latex Particles, Seragen Diagnostics Inc., Indianapolis, IN.

U. S. Department of Commerce
Malcolm Baldrige
Secretary

National Bureau of Standards
Ernest Ambler, Director

Appendix A

National Bureau of Standards

Certificate

Standard Reference Material 1965

Microsphere Slide (10-μm Polystyrene Spheres)

This Standard Reference Material (SRM) is intended for use as an optical microscopy measurement standard and teaching tool. The SRM is a microscope slide with two different groupings of 10-μm "space beads" permanently deposited on the surface and sealed in an air chamber (Figure 1). Each slide contains a few thousand microspheres. The microspheres are from SRM 1960, Nominal 10-μm Diameter Polystyrene Spheres, the first commercially available made-in-space product.

The microspheres in SRM 1965 are deposited in two different groupings: hexagonally ordered arrays and unordered clusters. The number average diameter of the particles in both groupings were measured by Center Distance Finding (CDF), an optical technique related to array sizing [1]. The certified values are:

	Number Average Diameter, μm	Uncertainty, μm
Hexagonal array	9.94	±0.04
Unordered clusters	9.89	±0.04

The uncertainty consists of both random and systematic errors, and includes sample-to-sample variability.

The number average diameter of the particles in the unordered clusters is the same as that of the microspheres in SRM 1960, from which the slides were prepared. The number average diameter of the spheres as measured in the hexagonal arrays is slightly greater due to a combination of three effects: (1) the measured mean diameter of spheres in hexagonal arrays is larger than the actual mean diameter by 0.04 μm due to the Kubitschek Effect (See SP 260-107 for detailed discussion); (2) the spheres are slightly swollen, by 0.03 μm, due to the processing required to produce the hexagonally-ordered arrays; and (3) the spheres are flattened at the contact areas by 0.02 μm.

The size distribution of the polystyrene spheres from which SRM 1965 was prepared, as determined by CDF [1], is a narrow Gaussian with a standard deviation of 0.9% (excluding particles with diameters not on the main peak). The number of undersized particles is negligible and the number of oversized particles is less than 1%.

The microsphere slide is expected to have an indefinite shelf life as long as the sealed cavity is not disturbed and the slide is handled with normal precautions and care.

Recommended Use: SRM 1965 can be used for a number of calibrations and exercises in micrometrology. The hexagonal arrays can be used as a two-dimensional microlength standard to replace calibrated "stage" micrometers. The hexagonal array can also be used for array sizing, diffraction experiments in crystallography, and for calibrating microscope image distortion and magnification. These applications, and a number of other exercises and techniques for optical micrometrology are described in detail in NBS Special Publication SP 260-107, which is supplied with the SRM.

January 15, 1987
Gaithersburg, MD 20899

Stanley D. Rasberry, Chief
Office of Standard Reference Materials

The technology necessary to produce these latex particles was developed by the Lehigh University and the National Aeronautics and Space Administration (NASA) during five shuttle missions in 1982 and 1983. The 10-μm particles in this SRM were manufactured in space aboard the Space Shuttle CHALLENGER during the NASA STS-6 mission, 4-9 April 1983. The particles were provided by NASA for certification by NBS as a Standard Reference Material to be made available to the scientific and technical communities.

The technical direction, production and physical measurements leading to the preparation and certification were provided by A.W. Hartman of the Precision Engineering Division.

Manufacture of the particles was carried out under the direction of J.W. Vanderhoff of the Lehigh University and D.M. Kornfeld of the National Aeronautics and Space Administration.

The technical and support aspects involved in the preparation, certification and issuance of this Standard Reference Material were coordinated through the Office of Standard Reference Materials by R.L. McKenzie.

[1] Hartman, A.W., Powder Technol, **42** (1985) 269.

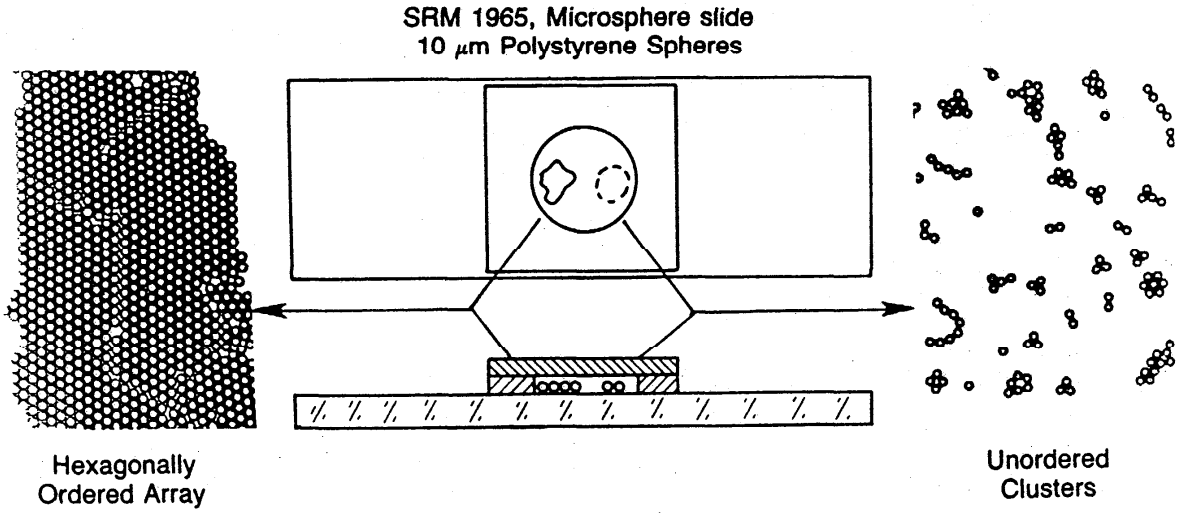

U. S. Department of Commerce
Malcolm Baldrige
Secretary

National Bureau of Standards
Ernest Ambler, Director

National Bureau of Standards

Certificate

Standard Reference Material 1960

Nominal 10 μm Diameter Polystyrene Spheres

(In Cooperation with the American Society for Testing and Materials)

This Standard Reference Material (SRM) is intended for use as a primary particle size reference standard for the calibration of particle size measuring instruments including optical and electron microscopes. The SRM is a suspension of polystyrene spheres in water at a weight concentration of about 0.4%.

The number average particle diameter was measured in air by Center Distance Finding (CDF), an optical technique related to array sizing [1]. The certified value is:

Number Average Diameter, μm	Uncertainty, μm
9.89	±0.04

The uncertainty consists of both random and systematic errors, and includes sample-to-sample variability.

The size distribution of the polystyrene spheres, as determined by CDF [1], is a narrow Gaussian with a standard deviation of 0.9% (excluding particles with diameters not on the main peak). The number of undersized particles is negligible and the number of oversized particles is less than 1%.

The material is expected to have at least a four-year shelf life when stored at room temperature, provided the cap on the vial is not removed. Care should be exercised to prevent contamination once the cap has been removed. Fifty μg/g of sodium azide was added as a biocide before the material was packaged.

Before sampling, manually shake and/or expose the SRM vial to ultrasonics until the spheres are uniformly distributed, then take a sample by squeezing a drop from the vial. Use filtered (0.4-μm pore size filter) distilled water for dilution. When electrolytes are used for electrical sensing zone counter measurements, first dilute the sample with water to prevent agglomeration.

The technology necessary to produce these latex particles was developed by the Lehigh University and the National Aeronautics and Space Administration (NASA) during five shuttle missions in 1982 and 1983. The 10-μm particles in SRM 1960 were manufactured in space aboard the Space Shuttle CHALLENGER during the NASA STS-6 mission, 4 - 9 April 1983. The particles were provided by NASA for certification by NBS as a Standard Reference Material to be made available to the scientific and technical communities.

The technical direction and physical measurements leading to certification were provided by T.R. Lettieri and G.G. Hembree of the Mechanical Production Metrology Division and A.W. Hartman of the Automated Production Technology Division.

Manufacture of the particles was carried out under the direction of J.W. Vanderhoff of the Lehigh University and D.M. Kornfeld of the National Aeronautics and Space Administration.

The overall coordination of the measurements by the cooperating laboratories was performed under the direction of R.C. Obbink, Research Associate, ASTM-NBS Research Associate Program.

The technical and support aspects involved in the preparation, certification, and issuance of this Standard Reference Material were coordinated through the Office of Standard Reference Materials by L.J. Kieffer.

[1] Hartman, A. W., Powder Technology (1985) (In Press).

April 4, 1985
Gaithersburg, MD 20899

Stanley D. Rasberry, Chief
Office of Standard Reference Materials

Cooperative determinations were performed in the following laboratories:

Climet Corporation, Redlands, California, L.D. Carver
Duke Scientific Corp., Palo Alto, California, S.D. Duke
Eastman Kodak Co., Rochester, New York, B.C. Wood
Food & Drug Administration, Minneapolis, Minnesota, G.S. Oxborrow
General Electric Co., Worthington, Ohio, E.J. Connors
Lehigh University, Bethlehem, Pennsylvania, J.W. Vanderhoff
National Aeronautics & Space Administration, Huntsville, Alabama, D.M Kornfeld
Pacific Scientific, Menlo Park, California, L.D. Carver
Particle Data Laboratories, Ltd., Elmhurst, Illinois, R. Karuhn

The following results are given for information only:

Method	Laboratory	Number Average Diameter (μm)	Standard Deviation of Distribution (μm)
Optical Microscopy	Duke	9.90	0.05
	FDA	10.215	0.176
	Kodak	9.93	- - -
Electron Microscopy	Lehigh	9.96	0.115
	Kodak	9.90	0.05
Sensing Zone	Duke	9.89	0.08
	G.E.	10.02	- - -
	Climet	10.08	- - -
	NASA	9.93	0.12
	Pacific Scientific	10.1	- - -
	Particle Data	9.94	- - -

Malcolm Baldrige
Secretary
National Bureau of Standards
Ernest Ambler, Director

National Bureau of Standards

Certificate

Standard Reference Material 1961

Nominal 30-μm Diameter Polystyrene Spheres

(In Cooperation with the American Society for Testing and Materials)

This Standard Reference Material (SRM) is intended for use as a primary particle size reference standard for the calibration of particle measuring instruments including flow-through counters and optical and electron microscopes. SRM 1961 is a suspension of polystyrene spheres in water at a weight concentration of about 0.5%.

The number average particle diameter was measured in air using Center Distance Finding (CDF), an optical technique related to array sizing [1]. Over 2000 particle diameters were measured with this technique. The certified value is:

Number Average Diameter, μm	Uncertainty, μm
29.64	±0.06

The uncertainty consists of both random and systematic errors, and includes sample-to-sample variability.

The value certified for the number average diameter was confirmed by one other measurement technique, Metrology Electron Microscopy (MEM). In this technique, which measures the particles in an ultra-high vacuum, the particles are individually scanned through a stationary electron beam while the position of the scanning stage is monitored by a stabilized helium-neon laser interferometer. A plot of secondary-electron intensity vs. stage position gives the particle diameter [2]. The result from MEM is 29.68 ±0.05 μm.

The size distribution of the polystyrene spheres, as determined by CDF, is Gaussian with a coefficient of variation of 0.8% (excluding particles with diameters not on the main peak). The material was precision sieved with a 33-μm diameter-opening electroformed sieve to remove oversized particles. As a result, the number of oversized outliers from the main peak is less than 1%; the same is true for the undersized outliers. A sphere is defined as an outlier if it's diameter is more than $4\sigma_D$ from the number average diameter of the main peak. The material is expected to have at least a four-year shelf life when stored at room temperature, provided the cap on the vial is not removed. Care should be exercised to prevent contamination once the cap has been removed. Fifty μg/g of sodium azide was added as a biocide before the material was packaged.

Before sampling, manually shake and/or expose the SRM vial to ultrasonics until the spheres are uniformly distributed, then take a sample by squeezing a drop from the vial. Use filtered (0.4-μm pore size filter) distilled water for dilution. When electrolytes are used for electrical sensing-zone measurements, first dilute the sample with water to prevent agglomeration.

The technology necessary to produce these latex particles was developed by Lehigh University and the National Aeronautics and Space Administration (NASA) during five space shuttle missions in 1982 and 1983. The 30-μm particles in SRM 1961 were manufactured in space aboard the space shuttle Challenger during the NASA STS-11 mission. The particles were provided by NASA for certification by NBS as a Standard Reference Material to be made available to the scientific and technical community.

The technical direction and physical measurements leading to certification were provided by A.W. Hartman, T. Doiron, G.G. Hembree, and T.R. Lettieri of the Precision Engineering Division of the National Bureau of Standards.

Manufacture of the particles was carried out under the direction of J.W. Vanderhoff of Lehigh University and D.M. Kornfeld of the National Aeronautics and Space Administration.

The overall coordination of the measurements by the cooperating laboratories was performed under the direction of R.C. Obbink, ASTM-NBS Research Associate.

The technical and support aspects involved in the preparation, certification, and issuance of this Standard Reference Material were coordinated through the NBS Office of Standard Reference Materials by R.L. McKenzie.

January 20, 1987
Gaithersburg, MD 20899

Stanley D. Rasberry, Chief
Office of Standard Reference Materials

[1] A.W. Hartman, **Powder Technology 46**, 109 (1986).

[2] S. Jensen, G. Hembree, J. Marchiando, and D. Swyt in **Semiconductor Microlithography VI, SPIE Vol. 275** (SPIE Bellingham, Wash., 1981).

Cooperative determinations were determined in the following laboratories:

Duke Scientific Corp., Palo Alto, California, S.D. Duke (also performed precision sieving).

Lehigh University, Bethlehem, Pennsylvania, J.W. Vanderhoff.

National Aeronautics and Space Administration, Huntsville, Alabama, D. Kornfeld.

Particle Data Systems, Elmhurst, Illinois, R. Karuhn.

The following results are given for information only:

Method	Laboratory	Number Average Diameter (μm)	Standard Deviation of Distribution (μm)
TEM	Lehigh	31.31	0.39
Electrical-sensing zone	Particle Data	30.16	0.78
	Duke	29.61	0.26
	NASA	29.09	0.37
Optical microscope	Duke	29.57	- - -

U. S. Department of Commerce
Malcolm Baldrige
Secretary

National Bureau of Standards
Ernest Ambler, Director

National Bureau of Standards

Certificate

Standard Reference Material 1691

Nominal 0.3 μm Diameter Polystyrene Spheres

(In Cooperation with the American Society for Testing and Materials)

This Standard Reference Material (SRM) is intended for use as a primary particle size reference standard for the calibration of particle size measuring instruments including electron microscopes. The SRM is a suspension of polystyrene spheres in water at a weight concentration of about 0.5%.

The number average particle diameter was determined by transmission electron microscopy (TEM) using SRM 1690 (nominal one-μm polystyrene spheres) to set the dimensional scale. The value reported is the mean of five independent data sets each consisting of over 100 measurements of 1-μm standard spheres and over 30 measurements of nominal 0.3-μm spheres.

Number Average Diameter, μm	Uncertainty, μm
0.269	±0.007

The uncertainty consists of both random and systematic errors, and includes sample-to-sample variability.

The value certified for the number average diameter was confirmed by one additional technique, quasielastic light scattering (QELS). In this technique, the average lifetime of the Brownian motion of the particles suspended in water is measured as a function of scattering angle. This gives a diffusion coefficient which can be used with the Stokes-Einstein relationship to yield the hydrodynamic particle diameter. The result from QELS was: 0.276 ±0.007 μm.

The size distribution of the polystyrene spheres, as determined by TEM, is narrow with a standard deviation less than 2% excluding outliers (particles with diameters not on the main peak). The number of small outliers is less than 1% and the number of large outliers is less than 0.5%.

The material is expected to have at least a four-year shelf life when stored at room temperature provided the cap on the vial is not removed. Care should be exercised once the cap has been removed to prevent contamination. Fifty ppm of sodium azide was added as a biocide before the material was packaged.

Before sampling, manually shake and/or expose SRM to ultrasonics until the spheres are uniformly distributed. Then take a sample by squeezing a drop from the vial.. Use filtered (0.1-μm pore size filter) distilled water for dilution. When electrolytes are used for electrical sensing zone counter measurements, first dilute the sample with water to prevent agglomeration.

The technical direction and physical measurements leading to certification were provided by T. Lettieri, G. Hembree, D. Gilsinn, and E. Marx of the Mechanical Production Metrology Division.

The overall coordination of the measurements by the cooperating laboratories was performed under the direction of R. Obbink, Research Associate, ASTM-NBS Research Associate Program.

The technical and support aspects involved in the preparation, certification, and issuance of this Standard Reference Material were coordinated through the Office of Standard Reference Materials by L.J. Kieffer.

May 1, 1984
Washington, DC 20234

Stanley D. Rasberry, Chief
Office of Standard Reference Materials

Cooperative determinations were performed in the following laboratories:

Brookhaven Instruments Corp., Ronkonkoma, New York, B. Weiner
Eastman Kodak Co., Rochester, New York, D. E. DeCann
Malvern Instruments, Malvern, England, F. McNeil-Watson
G. D. Searle and Co., Skokie, Illinois, M. Groves

The following results are given for information only:

Method	Laboratory	Number Average Diameter (μm)	Standard Deviation of Distribution (μm)
Electron Microscopy	Kodak	0.248	0.0026
Light Scattering			
Polarization Ratio	Kodak	0.273	0.003
Quasielastic	Kodak	0.272	
Quasielastic	Kodak	0.293	
Quasielastic	Brookhaven	0.273	
Quasielastic	Searle	0.282	0.0032
Quasielastic	Malvern	0.273	
Disc Centrifuge	Kodak	0.25	0.0027
Ultracentrifuge	Kodak	0.28	0.0029

U. S. Department of Commerce
Malcolm Baldrige
Secretary

National Bureau of Standards
Ernest Ambler, Director

National Bureau of Standards

Certificate

Standard Reference Material 1690

Nominal One-μm Polystyrene Spheres

(In cooperation with the American Society for Testing and Materials)

This Standard Reference Material (SRM) is intended for use as a primary particle size reference standard for the calibration of particle size measuring instruments including microscopes. The SRM is a suspension of polystyrene spheres in water at a weight concentration of about 0.5%.

The number average particle diameter was determined by measuring the light scattered by the polystyrene spheres suspended in water. The value used for the refractive index of polystyrene was $n(\lambda_{vac} = 632.99) = 1.588$. The diameter was determined from the best fit of Mie light scattering theory to the measured intensity versus angle.

Number Average Diameter, μm	Uncertainty, μm
0.895	± 0.008

The uncertainty includes both random and systematic errors.

The sample-to-sample variability (standard deviation) of the number average diameter, as determined on single drops taken from 20 vials (light scattering measurements of water suspensions and electrical sensing zone counter measurements), was found to be 0.0008 μm.

The value certified for the number average diameter was confirmed by two other measurement techniques. The first of these was by measuring the light scattered by individual spheres (8 were measured) levitated in air. In this technique both the diameter and refractive index are determined by the best fit to light scattering theory. In the second technique the average diameter was determined by optically measuring the row length of particles in two dimensional arrays formed by air drying. Scattering by individual particles: $(0.900 \pm 0.011\ \mu m)$. Optical array sizing: $(0.900 \pm 0.015\ \mu m)$.

The particle size distribution of the polystyrene spheres (as determined by measurements with a transmission electron microscope) is narrow with a standard deviation of about 0.009 μm, excluding small particles with diameters less than 0.6 μm (about 0.5%) and large single particles with diameters in the range of 2-6 μm (about 0.1%). A discordancy test based on the sample kurtosis was used at the 5% level for rejecting these particles [V. Barnett and T. Lewis, Outliers in Statistical Data, (Wiley, 1978) p. 101]. The particles are spherical with an average deviation from sphericity, $(D_{max} - D_{min})/D_{ave}$, of about 0.006. Measurements with an electrical sensing zone counter and by optical microscopy indicated that about 1.5% of the particles are agglomerated doublets.

The material is expected to have a four year shelf life when stored at room temperature provided the cap on the vial is not removed. Care should be exercised once the cap has been removed to prevent contamination.

Before taking a sample by squeezing a drop from the vial, manually shake and/or expose to ultrasonics until the spheres are uniformly distributed. Use filtered (0.2-μm pore size filter) distilled water for dilution. When electrolytes are used for electrical sensing zone counter measurements, first dilute the sample with water to prevent agglomeration.

The technical direction and physical measurements leading to certification were provided by G. Mulholland, T. Lettieri, G. Hembree, A. Hartman, and E. Marx of the Mechanical Production Metrology Division, with guidance on statistical analysis provided by K. Eberhardt of the Statistical Engineering Division.

The overall coordination of the measurments by the cooperating laboratories was performed under the direction of R. Obbink, Research Associate, ASTM-NBS Research Associate Program.

The technical and support aspects involved in the preparation, certification, and issuance of this Standard Reference Material were coordinated through the Office of Standard Reference Materials by R.K. Kirby.

Washington, D.C. 20234
December 22, 1982

George A. Uriano, Chief
Office of Standard Reference Materials

Cooperative determinations were performed in the following laboratories:

Air Products and Chemicals, Allentown, Pennsylvania, D.J. Nagy
Coulter Electronics Corp., Hialeah, Florida, R.T. Rodewald
Dow Chemical Co., Midland, Michigan, M.A. Langhorst
Duke Scientific Corp., Palo Alto, California, S.D. Duke
Eastman Kodak Co., Rochester, New York, B.C. Wood
General Electric Co., Worthington, Ohio, E.J. Connors
Pacific Scientific, Menlo Park, California, L.D. Carver

The following results are given for information only.

Method	Laboratory	Number Average Diameter (μm)	Standard Deviation of Distribution (μm)
Transmission Electron Microscope	Kodak	0.875	0.018
Opitcal Microscope Array Sizing	Kodak	0.895	- - - - -
Light Scattering			
Polarization Ratio	Kodak	0.900	0.067
Quasielastic	Kodak	0.93[a]	- - - - -
Quasielastic	Coulter	0.896[a]	- - - - -
Light Absorption	Pacific Scientific	0.87	0.030
Electrical Sensing Zone	Kodak	0.89[b]	0.023
Electrical Sensing Zone	Duke	0.90[b]	0.058
Electrical Sensing Zone	Coulter	0.87[b]	- - - - -
Electrical Sensing Zone	G.E.	0.89[b]	0.017
Disc Centrifuge	Kodak	0.91	0.046
Disc Centrifuge	Air Products	0.88	0.26
Hydrodynamic Chromatography	Dow	0.88[c]	- - - - -

[a] Type of average not specified.
[b] Number median diameter.
[c] Volume median diameter.

Appendix B

PROCESSING MATERIALS IN SPACE: THE HISTORY AND THE FUTURE

Roger Chassay*
Application Payload Projects Office
NASA Marshall Space Flight Center, AL

Bill Carswell**
Get Away Special Experimenter
San Jose State University, CA

Abstract

During the NASA Apollo missions to the Moon, several elementary experiments were performed to look at what happens when liquid materials are solidified without the effects of Earth's gravity. The results of these early experiments were very interesting, prompting NASA to conduct more sophisticated materials experiments at every opportunity. From the results obtained to date, many possibilities exist for new alloys, improved semiconductors, radiation detectors of impressive characteristics, sophisticated high technology glasses, new pharmaceutical products, and other novel materials. Can these possibilities be transformed into practical, cost-effective products for the benefit of mankind? The world's technologically leading countries are trying to find out.

Introduction

Long before materials science was developed in a sophisticated manner, surprising results were achieved by processing materials on Earth, despite the burden of gravity. Remarkably sophisticated swords were made by medieval blacksmiths; relatively mature 3000-year-old blast furnaces have been discovered in Africa; [1] and archeologists have unearthed iron implements in Egypt that appear to be about 5,000 years old. [2] Modern times have provided a rapid advance in materials technology, despite continued gravity effects. However, we are now preparing to slip the bonds of gravity and begin developing a true mastery over materials and the processes that bind them.

HISTORY

Although no one can say for sure who first suggested low-g materials processing, we know that in the 1780s William Watts of the United Kingdom obtained much better quality lead shot by using a freefall technique which he patented. [3] We also know that in the 1840s Joseph Plateau of Belgium suspended oil in a liquid of the same density, showing, among other important things, that the oil formed a perfect sphere when gravitational effects were removed. [4] The writings of the French novelist Jules Verne in the 1860s triggered more serious thought by Tsiolkovskiy of Russia in the 1880s. [5] Acknowledging that experiments by others had already shown that gravity has no effect on diffusion of fluids, Tsiolkovskiy's writings addressed important phenomena regarding liquids and gases in microgravity: 1) surface tension creates spherical shapes, 2) density driven segregation is absent, and 3) diffusion and surface tension become more prominent influences. He also suggested the use of asteroids as a source of raw materials for space bases and foresaw the creation of industrial activities in space.

Active interest in space processing began in the 1960s with a very few individuals taking the lead, principally Hans Wuenscher of NASA's Marshall Space Flight Center (MSFC). [6,7,8,9,10,11] These pioneers were convinced of the possibility of using low-g to overcome bouyancy driven convection and density gradient driven sedimentation. [12]

Drop Towers

Early microgravity materials research was done with the MSFC drop tower. [13] The drop tower allowed low-g experiments of a few seconds duration to investigate liquid spheres, hollow spheres, thin membranes, foaming, foams, liquid spreading, and liquid management.

Soyuz 6

The first Soviet orbital materials experiments were performed aboard the Soyuz 6 spacecraft. This work involved the use of an electron beam to melt and weld metals. [14]

Apollo

American scientists got their first chance to process materials in space when Apollo astronauts performed elementary experiments during their return trips from the Moon. Apollo 14 carried a composite casting apparatus which processed immiscible materials. These samples did not exhibit immiscible separation, the classic phenomena which occurs on Earth. Apollo 14 and Apollo 17 included fluid experiments which provided data on surface tension driven flow in low-g and indications of convection induced by the spacecraft and flight crew. Electrophoresis demonstrations performed on Apollo 14 and on Apollo 16 showed separations, although somewhat distorted, due to electro-osmosis. [1]

---

*Deputy Manager
Associate Fellow AIAA
**Student Member AIAA

Early Suborbital and Aircraft Flights

Two suborbital low-g flights were conducted in October 1971 and in January 1972 by NASA-MSFC to experiment with metallic foams and composite materials.[11] Short term, low-g sphere melting and sphere forming experiments by NASA-MSFC during KC-135 aircraft parabolic flight maneuvers began in 1972.

Skylab

The first sophisticated low-g materials experiments were conducted aboard the Skylab space station. Using experiments provided by scientists from the USA, Japan, and Belgium, astronauts completed fourteen materials experiments and also performed a group of nine enlightening materials science demonstrations. The results from the experiments and demonstrations were impressive: Crystals grew larger and were more pure; solid mixtures were more homogeneous; convection and sedimentation effects seemed negligible; amorphous materials were obtained in lieu of some crystals; and insights into low-g float zone mechanics were obtained. [15] A complete list of materials experiments and demonstrations carried out aboard Skylab is provided in figure 1.

SALYUT-4

Soviet scientists initiated a series of Salyut flight experiments in 1975 with two experiments: metal surface coating and the stability of rotating liquids.

Apollo-Soyuz

Also in 1975 a joint USA-Soviet mission, the Apollo-Soyuz Test Project (ASTP), was conducted with ten new experiments from American, Soviet, and West German scientists. This opportunity allowed continuation of some experiment areas investigated earlier on Skylab, as well as the initiation of investigations into entirely separate areas such as low-g electrophoresis. [16] A complete list of ASTP experiments is provided in figure 2.

Widespread Interest

By the mid-1970s there were enough reproducible and irrefutable low-g experiment results to spark the interest of most of the world's technologically leading countries. The USA intensified its efforts by adding a series of suborbital flights, called SPAR (Space Processing Applications Rocket).

Figure 1: SKYLAB MATERIALS EXPERIMENTS AND SCIENCE DEMONSTRATIONS

EXPERIMENTS	SKYLAB MISSION II	III	IV
MATERIAL PROCESSING FACILITY			
M551: Metals-Melting, R.M. Poorman, MSFC Astronautics Lab	X		
M552: Exothermic Brazing, J.P. Williams, MSFC Product Eng. Lab	X		
M553: Sphere-Forming, E.A. Hasemeyer, MSFC Product Eng. Lab	X		
MULTIPURPOSE FURNACE SYSTEM			
M556: Vapor Growth of II-VI Compounds, H. Wiedemeier, Rensselaer Polytechnic Institute	X		X
M557: Immiscible Alloy Compositions, J.L. Reger, TRW Systems	X		X
M558: Radioactive-Tracer Diffusion, A.O. Ukanwa, MSFC Space Science Lab	X		
M559: Microsegregation in Germanium, F.A. Padovani, Texas Instruments	X		
M560: Growth of Spherical Crystals, H.U. Walter, Univ. of Alabama	X		X
M561: Whisker-Reinforced Composites, T. Kawada, National Institute for Metals Research, Japan	X		X
M562: Indium Antimonide Crystals, H.C. Gatos, MIT	X		X
M563: Mixed III-V Crystal Growth, W.R. Wilcox, USC	X		X
M564: Alkali Halide Eutectics, A.S. Yue, UCLA	X		
M565: Silver Grids Melted in Space, A. Deruytherre, Katholieke Univ., Leuven, Belgium	X		
M566: Copper-Aluminum Eutectic, E.A. Hasemeyer, MSFC Product Eng. Lab	X		X
SCIENCE DEMONSTRATIONS			
Diffusion In Liquids	X		
Ice Melting	X		
TV 101 Liquid Floating Zone			X
TV 102 Immiscible Liquids			X
TV 103 Liquid Films			X
TV 105 Rochelle Salt Growth			X
TV 106 Deposition of Silver Crystals			X
TV 107 Fluid Mechanics Series			X
TV 117 Charged-Particle Mobility			X

The USSR began similar flights called MIR-2, [14] West Germany initiated a series of suborbital flights called TEXUS, and Japan conducted suborbital flights designated TT-500A.

The USSR continued its orbital materials experiment program by adding experiments on the Salyut 5, 6, and 7 missions. Salyut-5 experiments included metals melting and solidification, crystal growth, diffusion studies, and soldering demonstrations. Salyut-6 featured an electric furnace, a Czechoslovakian smelting experiment, and semiconductor manufacturing. [17]

A timeline showing the development of all these international programs is shown in figure 3.

Space Transportation System Experiments

When the USA introduced its Space Transportation System (STS) flights, materials scientists jumped at the opportunity to use this new research facility. The world's first space product, 10-micron latex spheres, was initially processed on STS-3 and later completed on STS-6. In the first four years of STS missions, USA scientists alone conducted over 35 low-g experiments. Figure 4 shows a list of the apparatus used for these microgravity science experiments. Many other low-g materials experiments were provided by other countries, including Austria, Belgium, Denmark, France, Great Britain, Italy, The Netherlands, Spain, Sweden, and West Germany.

FIGURE 2: ASTP EXPERIMENTS

ELECTROPHORESIS EXPERIMENTS

MA-011: Electrophoresis Technology
R.S. Snyder, MSFC Astronautics Lab
P.E. Bigazzi, State Univ. of New York
G.A. Barlow, Abbott Laboratories
M. Bier, Veterans Administration
MA-014: Electrophoresis (EPE)
K. Hannig, Max Planck Institute

MULTIPURPOSE FURNACE SYSTEM (MA-010)

MA-041: Surface Tension Induced Convection
R.E. Reed, Oak Ridge National Lab
MA-044: Monotectic and Syntectic Alloys
C.Y. Ang, Northrop Corp.
MA-060: Interface Marking In Crystals
H.C. Gatos, MIT
MA-070: Zero-G Processing of Magnets
D.J. Larson, Grumman Corp.
MA-085: Crystal Growth from the Vapor Phase
H. Wiedemeier, Rensselaer Polytechnic Institute
MA-131: Sodium Chloride-Lithium Fluoride Eutectic
A.S. Yue, UCLA
MA-150: Multiple Material Melting
USSR

COOPERATIVE EXPERIMENT

MA-028: Crystal Growth
M.D. Lind, Rockwell International

Accomplishments

The many accomplishments achieved to date can only be summarized in this brief paper, and, of course, a number of accomplishments have been omitted because we do not have access to the information. We have grouped the accomplishments by experiment types, by apparatus developments, and by unique ground facilities provided.

Bioprocessing

Protein Crystal Growth flight activities include one experiment in Spacelab 1 and four experiments in the Shuttle Middeck using a very simple, hand-held device. Since the purpose of these early experiments was to develop techniques for growing protein crystals in microgravity, no temperature control was provided. Nevertheless, some excellent crystals were grown, expecially on STS-61C when the experiment was performed by Payload Specialist, U.S. Congressman Bill Nelson. Several crystals yielded very high resolution x-ray diffraction patterns, indicating a well-ordered crystalline structure. Analysis of these crystals is still in progress to see how they compare with the best crystals grown on Earth.

In addition to these flight experiments, the synergism between the various disciplines involved in the project has produced new insights into the growth of protein crystals and improved Earth-bound growth techniques.

Laboratory activities include the investigation of lysozyme crystal growth kinetics and development of a growth process model which provided data used to determine the relative role of transport and interfacial kinetics in lysozyme crystal growth. New techniques have been developed and used to determine the phase diagrams for various protein crystal growth conditions. We have also crystallized tryptophan synthase from E. coli, a protein that had not been previously crystallized.

Relative growth rate measurements of human serum albumin and sucrose clearly show that the crystal growth rate is greatest in the direction perpendicular

to the density-driven convective flow, due to the replenishment of source material at the growth interface.

Electrophoresis activities have determined parameters affecting sample stream distortion in ground- and space-based continuous flow electrophoresis devices. They have also established the parameters controlling buoyancy-driven flows in wide gap, ground-based continuous flow electrophoresis devices. A ribbon-like flow distortion phenomenon has been observed in ground-based electrophoresis-type flow chambers which is not fully understood. A series of ground and flight experiments is planned to find out if the distortions are related to buoyancy effects.

A moving wall continuous electrophoretic separator has been built which is uniquely adapted to space-based separations. This technique increases throughput and resolution for a multicomponent sample and represents a substantial improvement over conventional free-flow electrophoresis.

McDonnell Douglas used its chamber o STS-6 and -7 to determine the effects of sample concentration and conductivity on separation performance. Large distortions in the sample stream were found when there was a mismatch between sample and buffer conductivity. This distortion had not been revealed in previous ground-based work because the space experiment allowed the first use o sample concentrations high enough to hav mismatched conductivities.

Various zeta potential coatings have been developed to control electroosmotic flow in electrophoresis devices.

Low-G Isoelectric Focusing experiments (separation into pH bands) have been conducted, revealing unexpecte flow distortions. An improved electro-osmotic coating has been developed which should allow this promising method to be developed into a usable process for separating cells and macromolecules.

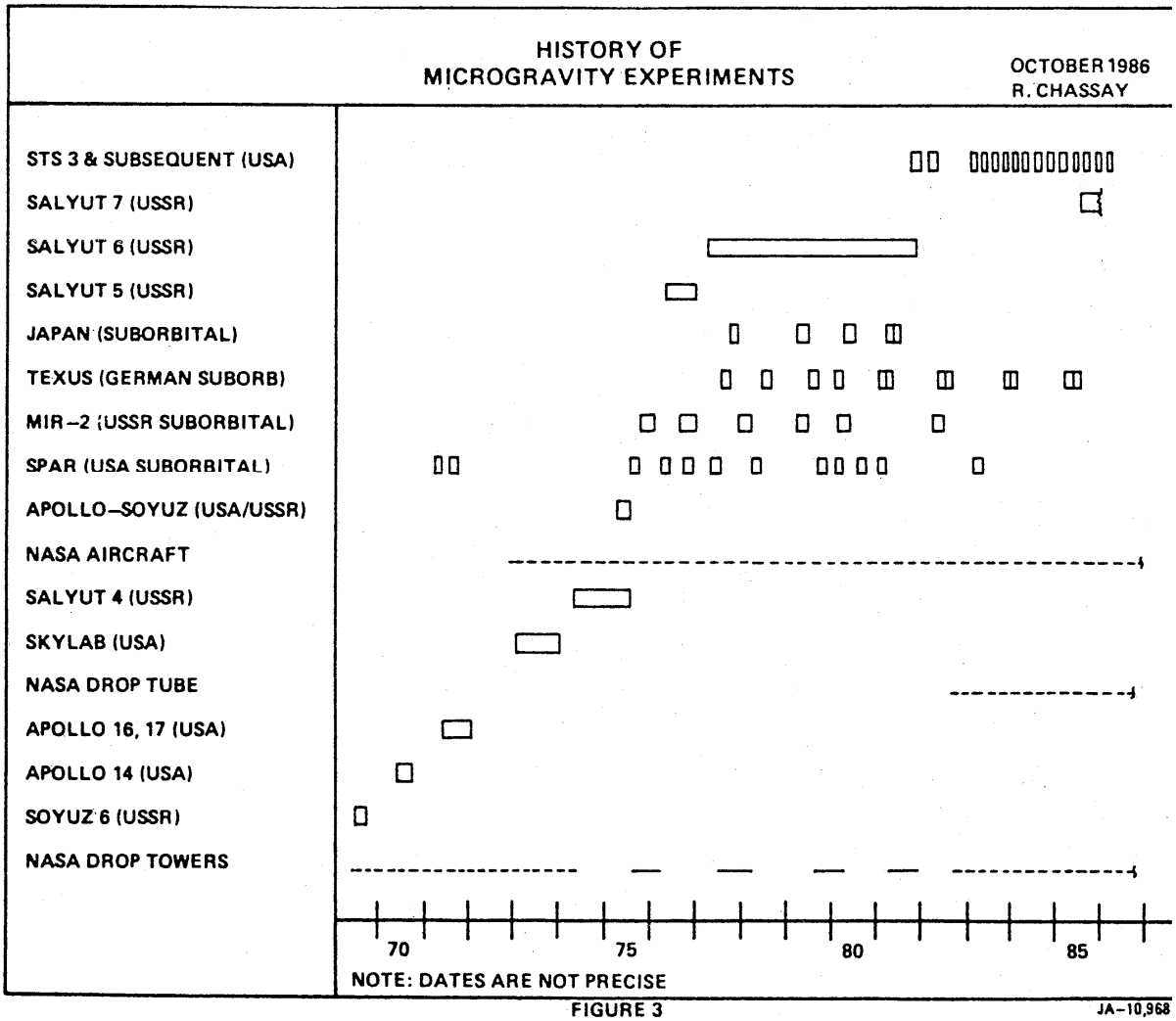

FIGURE 3

JA–10,968

Phase Partitioning experiments have been conducted to find alternate methods of controlling the partitioning of the two polymer aqueous phases used in the separation of biological cells. When gravity drives the separation of the mixed phases, shear forces from the rapid fluid movement detach the biologicals being separated from their respective phases. This degrades the efficiency of the technique and requires many repetitive cycles to obtain reasonable purity. These shear forces are greatly reduced in low-g.

Immunoaffinity phase partitioning was demonstrated at NASA-MSFC, indicating the potential of this technique for highly specific cell separations.

A Monodisperse Latex Reactor (MLR) has been flown on five shuttle missions, beginning with STS-3, and has successfully manufactured monodisperse polystyrene latex during these flights by means of seeded emulsion polymerization.

The MLR produced the world's first space product to be sold on Earth: 10-micron latex particles. These tiny spheres were certified and placed on sale by the U.S. National Bureau of Standards (NBS) on July 17, 1985, as Standard Reference Material (SRM #1960). The sale price was $384 per vial of 30 million microspheres, and, within one year of being released for sale, almost half of all the vials had been sold.

The world's second space product, the 30-micron latex spheres manufactured on STS-11, has also completed certification by NBS and will go on sale as SRM #1961.

Electronic Materials

Semiconductor Crystal Growth activities have resulted in improved sample containers which reduce undesirable grains at the container wall through the use of a thin non-wetting graphite coating on the inner surface of the quartz ampoule.

Thermal models of crystal growth furnaces have been greatly enhanced by including radiation heat transfer. This

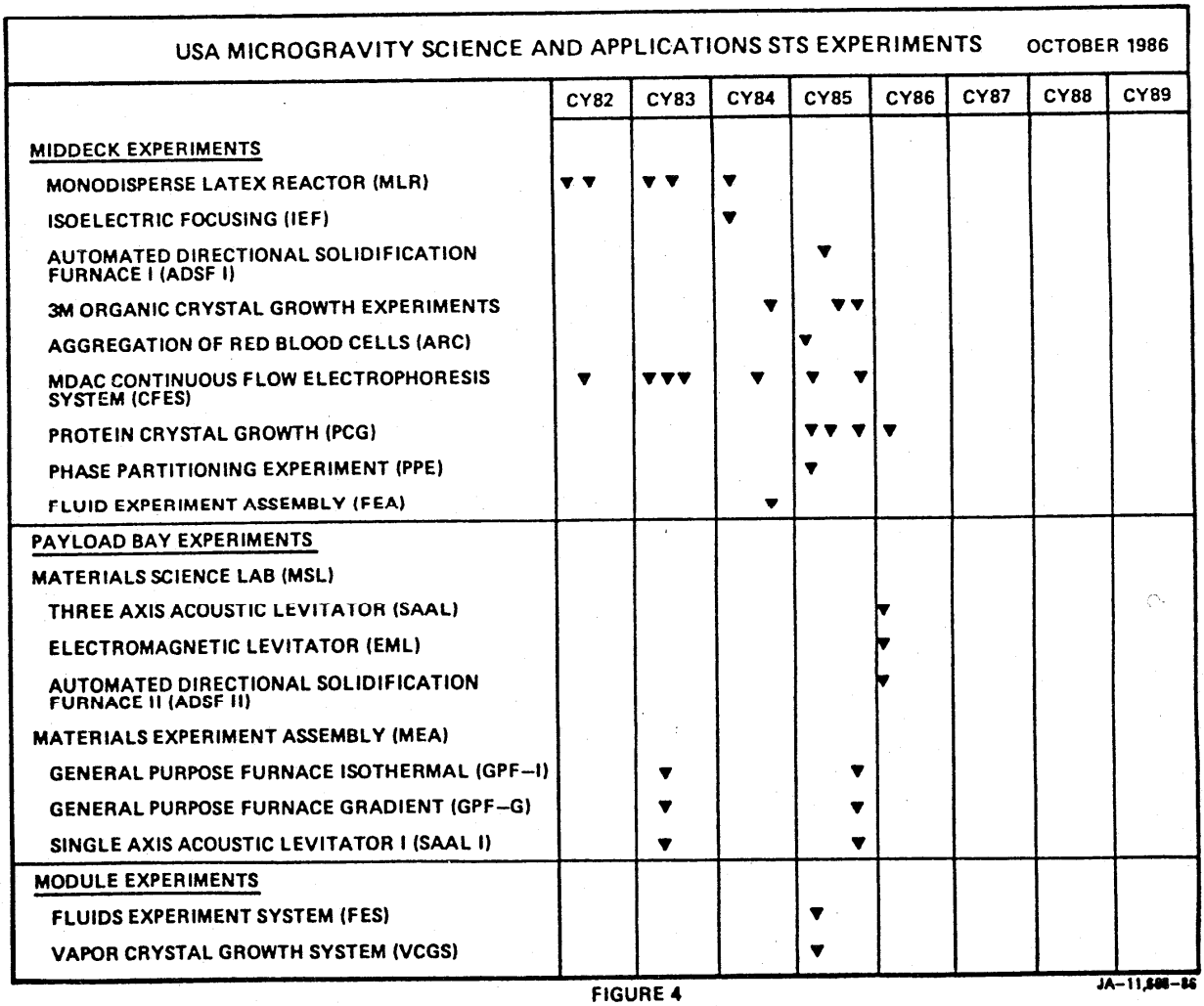

FIGURE 4

is required for accurate prediction of the growth interface shapes when the liquid is transformed to solid crystal.

New insight has been obtained into the influence of convection in crystal growth and on the difficulty of suppressing convective flows, even in microgravity. It now appears necessary to combine strong magnetic fields with microgravity in order to grow large crystals in a diffusion-controlled environment. The lines of force of a sufficiently strong magnetic field create an induction drag across a conductive melt. This drag dampens motion across the magnetic lines of force, cancelling out surface tension driven convective flows. [18] This technique for suppressing convection has gained widespread use in terrestrial semiconductor growth processes, especially by the Japanese. [19]

Solution Crystal Growth activities have included the development of an optical technique, using laser interferograms and shadowgraphs, to directly observe the growth or dissolution of a crystal with high precision measurement of solubility at various concentrations. This technique successfully supported the Triglycine Sulfate experiment on Spacelab-3 and is now being applied to solution growth of non-linear optical materials, which appear to exhibit improved characteristics when produced in low-g.

The Triglycine Sulfate Experiment on Spacelab-3 successfully produced two detector crystals grown for the first time in microgravity. This marks a major milestone in growth of crystals from a solution. The experiment also provided hundreds of holograms for use in analyzing the distribution of solute in the solution. Preliminary analysis of the holograms reveal that diffusion-controlled growth conditions prevailed throughout most of the mission because of the very low steady accelerations of less than 10^{-6} g, despite the fairly large 10^{-3} g frequency accelerations (g-jitter) caused by internal motions.

Vapor Crystal Growth Experiments in the Materials Experiment Assembly (MEA) flown on the Space Shuttle produced some surprising and unexpected results. The vapor-growth flight samples had loose, web-like structures of large platelets. These experiments also produced thin crystals that grew in the gas atmosphere instead of on the ampoule wall. Some of the crystals were significantly larger than those produced on Earth. For example, one of the space-grown crystals was about 20mm x 10mm. Also, the experiment samples make it very clear that the more uniform microgravity growth conditions have a beneficial effect on surface and bulk morphology.

The flight experiments have provided excellent agreement with theory for four different flux vs. pressure points.

The Mercuric Iodide Experiment, performed using a nuclear detector material aboard Spacelab-3 (SL-3) in 1985, was developed to grow single crystals in a microgravity environment. Much new and useful information was obtained even prior to flight during ground-based research. The flight results provided a benchmark against which comparison to Earth crystals can be made. The following data, while preliminary and to be regarded with some degree of caution, is very encouraging: Electron mobilities, important for detector performance, were measured in a sample from the space crystal and found to be twice as high as any ever reported for a terrestrially grown crystal. Furthermore, hole mobilities appeared to be as much as seven times higher than in Earth-grown crystals.

Electronic and Electro-Optical Materials. The first direct experimental evidence has been obtained at MSFC for the transitions from semiconductor to metallic behavior in Mercuric Telluride and in Mercuric Selenide, i.e. that the melt has almost an order of magnitude more conductivity than the solid. Additionally, the importance of gravity-driven convection has been empirically established in the compositional redistribution which occurs during casting of HgCdTe alloys -- the material of choice for long wavelength infrared detector applications. A thermal model of Bridgman growth of Mercury Cadmium Telluride has been developed which predicts interface shapes for various furnace temperature profiles This is necessary for the optimization of science return from low-g experiments.

Organic Thin Films and Crystalline Solids were grown via the physical vapor transport (PVT) method by 3M on STS-51I. This was the first known attempt to grow organic crystals and thin films by vapor transport in microgravity. Each of the solid samples was vaporized, then allowed to recondense onto a cooler substrate. Initial analysis of the samples has shown very well defined substrate deposits, both thick and thin film, in all nine of the flight ampoules. This demonstrates clear dependence of film formation on the molecular weight of the buffer gas. [20]

Metals and Alloys

Deep Undercooling: A 105-meter drop tube facility is being used at NASA MSFC to provide very deep undercooling of more than 500 degrees C during containerless freefall processing of Niobium-Germanium Niobium-Platinum, and Niobium-Silicon alloys. Analyses have revealed a non-equilibrium eutectic phase as well a

an amorphous area in the Nb-Ge samples. Drops of ten different samples of pure metals also have been significantly undercooled and will be used to test current nucleation theories.

Magnetic Materials have undergone suborbital and orbital experiments which indicate that convection has been effectively damped in low-g and diffusion-controlled growth has been achieved. Increases in permanent magnetic properties have been observed which approach the theoretical maximum.

Immiscible Materials have been studied in depth in view of the possibility of overcoming the separation tendencies inherent in the gravity environment. Several low-g phenomena have been identified which must be overcome to achieve completely homogeneous mixtures of immiscible alloys. Interfacial tensions induce a strong tendency toward massive phase separation in microgravity. Thermal gradients induce liquid droplets of one phase to migrate toward the center of the melt as the alloy cools, resulting in the surrounding of one material by the other. Interfaces between vapors and liquid surfaces contribute to surface tension-driven convective flows, causing phase separation. The interaction of the droplet phase with the crucible walls causes droplets to adhere to and spread on the container wall, thereby inhibiting thermocapillary droplet migration. This may be avoided by proper selection of crucible material.[21]

Metal Solidification Research experiments conducted in space and in low-g aircraft parabolic flights have developed new knowledge of solidification mechanisms and the basic structure of metals and alloys. Iron-graphite alloy studies have revealed the effects of gravity on the uniformity of the crystalline structure in cast iron. Unexpected effects, such as changes in dendrite arm spacing, have been discovered in microgravity. Studies of superalloys and monotectic alloys have contributed to an understanding of the basic structure of these materials and have given important clues as to how this information may be used in ground processing of these materials.

Glasses

Reluctant Glass-Forming Materials studies have shown that the possibility of producing important new amorphous materials can be enhanced through the use of acoustic containerless processing. However, in the absence of a container the surface "skin" (or oxides) of some materials has been a source of heterogeneous nucleation. Time, temperature, and transformation data (TTT curves) have been otained for a number of glass-forming systems to determine the cooling rates required to form a glass. Several different nucleation mechanisms have been identified, including heterogeneous nucleation, caused by small particles in the melt, on container walls, or on the melt spinning substrate, and dynamic nucleation, caused by mechanical shear. In order to determine the precise impact of homogeneous nucleation on glass formation, it will be necessary to determine the values and temperature dependence of the crystal melt interfacial tension, the driving free energy, and the atomic mobility.

Containerless Glass Formation experiments have been conducted in microgravity using the single axis acoustic levitator/furnace (SAAL). For the first time, liquid specimens were successfully levitated in space at high temperatures: 1250 to 1500 degrees C. Two glass forming samples, soda-lime-silica and calcia-gallia-silica, were melted and cooled to glass while levitated in space. The result was clear evidence of a two- to three-fold increase in the glass formation tendency (via a comparable decrease in minimum cooling rate for glass formation) in calcia-gallia-silica solutions.

New Space Processing Apparatus

Although many new apparatus have been developed, we will briefly cover only the U.S. apparatus. [3]

NASA-MSFC Apparatus

The Fluid Physics System (also called the Fluids Experiment System) is a highly sophisticated apparatus capable of conducting low-g experiments in fluid dynamics, bubble behavior, solution crystal growth, and nucleation and ripening phenomena. The system includes a laser holographic capability and 22 temperature controls with accuracies to 0.01 degrees C. It was utilized on the Spacelab-3 mission in 1985 to produce the two Triglycine Sulfate crystals for detector devices. The system also includes a schlieren and shadowgraph capability to provide multiple optical modes for fluid dynamics analyses.

Holographic Imaging of Crystal Growth techniques have been developed and applied to the study of solution crystal growth. The holograms produce high resolution images of the growth process and the interaction of the crystal with its surrounding solution. These frames can then be analyzed by interferometric methods at a later time. This has been very useful for both ground-based studies and flight experiments. Development is underway of a two-color holographic system, which can distinguish between the effects of concentration gradients and temperature gradients.

A Vapor Crystal Growth System was demonstrated on Spacelab-3. The system provides precision temperature repeatability and stability to within 0.05 degrees C. It also provides continuous viewing of crystal growth, which allows critical adjustments to be made in real-time to optimize growth conditions. The system has a capability to interrupt the growth process, allowing anomalous growth to be eliminated in real time by vaporization prior to proceeding with the crystal growth.

Laser Scattering Microscope methods measure, in a non-destructive manner, the distribution of defects in transparent solution-grown crystals. Laser light is focused and scanned throughout the crystal. The light scattered, due to defects, is detected and recorded by a microscope/computer system. This system is helping determine the quality of space-grown crystals.

General Purpose Microgravity Furnaces have been developed to study the basic nature of low-gravity metal solidification. The understanding of these processes, in turn, helps improve manufacturing techniques on Earth.

A Multiple Experiment Processing Furnace is being planned to process a large number of metal and semiconductor samples during each flight. The primary feature separating this new generation furnace from previous models is the ability to manually or automatically change samples during a mission.

Directional Solidification Furnaces have been developed to study the formation of crystal structures and the solidification process in metals and alloys in low-g.

The Advanced Automated Directional Solidification Furnace engineering prototype has been developed and tested. This highly modular prototype furnace features a controlled gradient region consisting of a series of microprocessor-controlled, thin trim heaters in the vicinity of the solidification interface. These trim heaters can reduce radial temperature gradients near the solid-liquid interface, resulting from changes in thermophysical properties as the melt crystallizes, e.g. changes in thermal conductivity or emissivity. Such control is required for microgravity crystal growth of electronic and electro-optical materials, such as lead-tin-telluride, mercury-cadmium-telluride, gallium-arsenide, etc.

Containerless Processing Apparatus have been developed for microgravity processing of experiment samples which are adversely affected by contact with a container. These apparatus, the 1300-degree-C NASA Electromagnetic Levitator, the 1600 degree C Single Axis Acoustic Levitator, and the Three Axis Acoustic Levitator (3AAL), have all been demonstrated in flight. These apparatus are setting the stage for development of advanced containerless processing systems to meet our Space Station requirements.

NASA Goddard Space Flight Center Apparatu

Get Away Specials: NASA-GSFC's Get Away Special (GAS) program was first introduced at an AIAA meeting in 1976, at which time the first reservation was made. Since then, 53 experiments have flown on 13 Space Shuttle missions, and 458 reservations remain unflown. The program has acheived a high level of respectability because of its effectiveness in involving persons and organizations in space research that otherwise would never have had such an opportunity. Many GAS experimenters are now employed by NASA, its contractors, and associated universities. The GAS program is clearly the least expensive, most straightforward means available of performing small-scale materials science investigations aboard the Space Shuttle.

Unique Ground Facilities

NASA has developed ground facilities to aid in preparing highly productive space experiments, since access to space is still quite limited and space experiment opportunities are not readily available.

NASA-MSFC Facilities

A Ground Control Experiments Laboratory has been set up and used extensively for developing the flight protocol for many crystal growth and metallurgical experiments. This laboratory produces control specimens for comparison with low-g experiment samples.

A Holographic Ground Facility has been completed to reconstruct the holographic images recorded in space, primarily from the Fluids Experiment System. Various optical techniques are being applied to the reconstructed images to extract the fluid and crystal growth information so that the flight environment can be related to the resultant crystal growth.

105-Meter Drop Facilities, as mentioned earlier, have been developed to allow quick-reaction, low-cost, short duration (approx. 4 seconds) periods of processing in low-g for investigators who need precursory experiments prior to Shuttle experiments.

KC-135 and F-104 Aircraft have been modified for conducting tests using low-gravity parabolic flights to assess experiment apparatus which cannot be

calibrated or evaluated in one-g. These flights are also used for conducting experiments requiring only short periods of low gravity (approx. 15-40 seconds).

A Semiconductor Characterization Facility has been established for crystal growth and characterization of electronic and electrooptical materials to support space-based crystal growth of these technologically important materials. The laboratory includes extensive facilities for the purification of starting materials, casting of the desired alloys, and crystal production by melt, solution, and vapor growth methods. Facilities for the slicing, polishing, and etching of samples for characterization are also provided. The laboratory includes facilities for the compositional, metallurgical, electrical, and optical characterization of the materials, including elevated and cryogenic temperatures. Activities in the laboratory include theoretical and numerical modeling of the heat and mass transport phenomena involved in the various growth processes to optimize processing parameters for flight crystal growth experiments.

NASA Lewis Research Center Microgravity Materials Science Laboratory

The Microgravity Materials Science Laboratory (MMSL) contains functional duplicates of some experiment equipment flown on the Space Shuttle. It is designed to give visiting scientists a chance to familiarize themselves with flight hardware. The current focus of the laboratory is on metal and alloy solidification and crystal growth research, but capabilities are being expanded to provide equipment for research in polymers, ceramics, and glasses. The following is a list of apparatus available or soon to be available for use at the MMSL.

- -General Purpose Furnace
- -Electromagnetic Levitator
- -Instrumented Drop Tube
- -Undercooling Furnace
- -Bulk Undercooling Furnace
- -Transparent Directional Solidification Furnace
- -High Temperature Directional Solidification Furnace
- -Isothermal Dendrite Growth Apparatus
- -Crystal Growth Furnace
- -Single Axis Acoustic Levitation Furnace

THE FUTURE

Planned for launch by the end of 1992, the U.S. Industrial Space Facility (ISF) will support commercial research, development, and manufacturing in space. We will also see the development of the Space Station by the U.S., Canada, Japan, and the European Space Agency (ESA). When these and other new space platforms become available, we will see a dramatic increase in low-g research time. The ensuing contributions to the field of microgravity materials science should be enormous.

The Industrial Space Facility (ISF) is being developed by Space Industries, Inc. and Westinghouse. It will be launched by the Space Shuttle into low Earth orbit for commercial activities. The ISF is expected to provide up to 12 Kw of power to its users, along with appropriate systems for power storage, heat dissipation, attitude control, and data management. Man-tended processing will be accomodated in a shirtsleeve environment and resupply operations are planned from the Space Shuttle.

The U.S. International Space Station will support a wide variety of experiments near the station's center of gravity, where there will be the lowest practical residual accelerations. Electrical power of 12 to 59 Kw is expected to be available for experimental use. Limited on-orbit sample characterization will be provided. Some of the several new research facilities that may be developed for the Space Station include:

- -Small Bridgman Growth Facility
- -Large Bridgman Growth Facility
- -Bulk Crystal Growth Facility
- -Metals and Alloys Solidification Facility
- -Float Zone Crystal Growth Facility
- -Electroepitaxial Crystal Growth Facility
- -Vapor Crystal Growth Facility
- -Solution Crystal Growth Facility
- -Protein Crystal Growth Facility
- -Organic and Polymer Crystal Growth Facility
- -Containerless Processing Facility
- -Optical Fiber Pulling Facility
- -Fundamental Science Facility
- -Combustion Science Facility
- -Cloud Microphysics Facility
- -Electrokinetic Separation Facility
- -Geophysical Fluid Flow Facility
- -Ultra-Vacuum Facility

Each of these new apparatus will provide a significant advancement in capability beyond presently used low-g apparatus. Other apparatus could be added to the above list of development candidates as the Space Station availability date gets closer.

To provide inputs to the design of the Space Station, studies have been performed to indicate requirements for Space Station resources. This was accomplished by grouping about 25 typical low-g apparatus, both new and existing, which would time-share these resources,

e.g. biotechnology, crystal growth, solidification, fluids, combustion, containerless processing, etc. Similar assessments have determined typical types of laboratory equipment which would be required, assuming on-orbit sample characterization is performed. [22]

The USSR Mir Space Station, along with its accompanying microgravity science facilities, has been offered for use by European scientists. Mir provides 7-10 Kw (and may eventually provide as much as 15 Kw) of power for experiments. It also provides materials science furnaces with operating temperatures of from 1000 to 1500 degrees C. [23]

The European Retrievable Carrier EURECA is a free-flying space platform being developed by the European Space Agency. This platform will support sophisticated materials processing with modest power levels, i.e. 1000 watts. Several low-g apparatus have already been developed specifically for use on EURECA.

Technology Advancements are needed in several key areas. NASA and other organizations are assessing particular advanced technology needs that will allow full utilization of the new apparatus and new space facilities such as the Space Station and the ISF. For example, certain low-g processes are expected to require lower residual accelerations than the Space Station can provide. Therefore, isolation systems may be utilized on the Space Station which use, for example, an electromagnetic field to protect these highly sensitive experiments or processes from g-jitter and other harmful accelerations above 10^{-6} g. Other items of new technology which may be necessary are ultra-high temperature furnace modules, high temperation calibration systems, two-color holographic interferometry, superconducting magnets for on-orbit suppression of fluid motion, inflight x-ray analysis equipment, and measurement systems for non-invasive analysis of the physical and chemical properties of high temperature molten materials.

Conclusions

Twenty years ago, only a very few individuals had even vague notions of what could be accomplished with low-g processing. Today, low-g processing is widely known in every technologically advanced country and is a rapidly emerging new technology, well-supported by hundreds of government and private organizations. Obviously the future cannot accurately be predicted, but it is safe to say that exciting prospects exist for marvelous new materials to be developed in space or, perhaps more importantly, for low-g research to point the way for improved Earth-based processing of materials.

REFERENCES

[1] Naumann, Herring, "Materials Processing in Space: Early Experiments" NASA SP-443, 1980.

[2] Huntsville Times, October 6, 1986.

[3] Feuerbacher, Hamacher, and Naumann, "Material Sciences in Space," March 1986.

[4] Dictionary of Scientific Biography, Volume XI, 1975.

[5] "Selected Works of K.E. Tsiolkovskiy," NASA TT F-237, Volume II, September 1965.

[6] Wuenscher, H.F., "Low and Zero-G Manufacturing in Orbit," AIAA Paper 67-842, October 1967.

[7] Wuenscher, H.F. "Unique Manufacturing Processes in Space Environment," Seventh Space Congress, April 1970.

[8] Siegret, Petrash, and Otto, "Time Response of Liquid-Vapor Interface After Entering Weightlessness," NASA TN D-2458, 1964

[9] Aviation Week & Space Technology, pp. 63-69, April 7, 1969.

[10] Wuenscher, H.F., "Space Manufacturing Unique to Zero Gravity Environment," NASA TM Report #53851, July 1969.

[11] Yates, Yost, "Investigations of Stability of Bubbles in Plain and Fiber-Reinforced Metal, Melted and Solidified in a Near-Zero-G Environment," NASA TM X-64665, October 1972.

[12] McKannan, "The Growth of Materials Processing in Space - A History of Government Support for New Technology," NASA-MSFC Space Science Laboratory Preprint Series No. 83-130, August 1983.

[13] Steurer, "Revised Free-Fall Experiment Program for 80- and 300-Foot Towers," FFX Report #3, February 1970.

[14] Avduyevsky, Grishin, Leskov, Polezhayev, and Savitchev, "Scientific Foundations of Space Manufacturing," 1984.

[15] Stuhlinger, "Materials Processing in Space: A Look Toward the Future," Astronautics and Aeronautics, May 1975.

[16] Naumann, "Materials Processing in Space: A Program Overview," June 1978.

[17] Dooling, "The Space Factory" from Space Technology, Gatland ed., Harmony Books, 1981.

[18] Langlois, W.E., "Buoyancy-Driven Flows In Crystal-Growth Melts," Ann. Rev. Fluid Mech., 1985, pp. 191-215.

[19] Carruthers, personal communications.

[20] Debe, Cook, Poirier, Follett, Miller and Spiering, "Vacuum Outgassing and Gas Phase Thermal Conduction of a Microgravity Physical Vapor Transport Experiment," 10th Annual International Vacuum Congress, October 27-31, 1986.

[21] Gelles, Markworth, and Mobley, "Low Gravity Experiments on Liquid Phase Miscibility GAP (LPMG) Alloys - Materials Experiments Assembly (MEA)," Fourth European Symposium on Materials Science Under Microgravity, ESA-SP191, June 1983.

[22] "Microgravity and Materials Processing Facility Study," Teledyne Brown Engineering Report, September 1985.

[23] Space Business News, October 20, 1986.

THE FIRST PRODUCTS MADE IN SPACE: MONODISPERSE LATEX PARTICLES

J. W. Vanderhoff*, M. S. El-Aasser, F. J. Micale,
E. D. Sudol, C.-M. Tseng, and H.-R. Sheu
Emulsion Polymers Institute and Departments
of Chemistry and Chemical Engineering
Lehigh University
Bethlehem, Pennsylvania 18015

and

D. M. Kornfeld
George C. Marshall Space Flight Center
Huntsville, Alabama 35812

Abstract

Twenty monodisperse polystyrene latexes were made by seeded emulsion polymerization in the MLR-SEP flight hardware on the STS-3 and STS-4 flights of the Columbia and the STS-6, STS-7, STS-11 flights of the Challenger. Two polymerizations were small-particle-size controls; eighteen were of large particle size. Of these, six failed: four on STS-4 owing to malfunction of the flight hardware; one on STS-6 owing to a broken wire; one on STS-11 owing to a broken stirrer shearpin. Nine monodisperse latexes of 4-30 μm size had narrower partiicle size distributions than the ground-based controls. The 10 μm STS-6 latex and the 30 μm STS-11 latexes were accepted by the National Bureau of Standards as Standard Reference Materials, the first products made in space for sale on earth. The polymerization rates in space were the same as on earth within experimental error. The flight polymerizations produced only negligible coagulum; the ground-based control polymerizations produced increasing amounts with increasing particle size, so that these controls were discontinued after the STS-7 experiments. These results confirmed the original rationale of the experiments that polymerization in space would give more uniform large-particle-size monodisperse latexes with less coagulum by: 1. the better uniformity of all 5 μm or larger flight latexes; 2. the more perfect sphericity of the 10 and 30 μm flight particles; 3. the smaller number of offsize larger particles; 3. the negligible amounts of coagulum; 4. the broadening of the particle size distribution and the formation of larger offsize particles during the completion on earth of the polymerization of the partially converted STS-4 flight latexes.

Introduction

Since 1947 monodisperse polystyrene latexes have found wide application as calibration standards and other scientific uses.[1] Series of monodisperse latexes were prepared by seeded emulsion polymerization, i.e., by polymerizing monomer in a previously prepared monodisperse latex;[2,3] the particle size distribution is self-sharpening at small particle sizes.[4-6] The emulsifier concentration is critical: too little results in flocculation of the latex; too much results in nucleation of a new crop of particles.[6]

The first series of monodisperse latexes ranged in average diameter from 88 nm (standard deviation σ 8.0 nm) to 340 nm (σ 5.2 nm) to 1171 nm (σ 13.3 nm).[3] The standard deviations included not only the width of the particle size distributions, but also the errors involved in measuring the individual particle images of the electron micrographs and the difference in magnification from one exposure to another.[3] A later series showed improved monodispersity: the average particle diameters ranged from 91 nm (σ 5.8 nm) to 176 nm (σ 2.3 nm) to 1100 nm (σ 3.5 nm) to 2020 nm (σ 13.5 nm).[7]

Even larger sizes were prepared in the laboratory, i.e., as large as 5.6 μm in 100-gm quantities and 10-12 μm in much smaller quantities.[8] The quantities were small because the polymerizations produced increasing amounts of coagulum, giving complete coagulation of the 10-12 μm sizes. The range of emulsifier concentrations that gave neither coagulum nor a new crop of particles was relatively broad at submicroscopic particle sizes,[6] but narrowed with increasing size, so that duplicate polymerizations yielding 2 μm particles gave either stable latexes contaminated with a new crop of smaller particles or relatively unstable monodisperse latexes.[8]

Particles larger than 2 μm show little or no Brownian motion; polystyrene (1.050 gm/cc) seed latex particles swollen with styrene monomer (0.905 gm/cc) cream and the polymerized particles settle. Of course, creaming or settling of the particles can be offset by stirring, which is always used in emulsion polymerizations; however, the large, soft, sticky monomer-swollen particles are sensitive to mechanical shear and thus are easily coagulated by too-vigorous stirring. The result is that the larger the particle size, the faster must be the stirring to avoid creaming and settling; however, too-fast stirring gives mechanical coagulation, so that it is difficult to prepare large-particle-size latexes without excessive coagulum.

In space, the particles would show no

*Professor, Department of Chemistry
Member AIAA

tendency to cream or settle; therefore, the polymerization would be stirred only well enough to ensure good heat transfer and mixing (for the latex to be monodisperse, each particle must have the same temperature-time history, as the rate of polymerization increases with increasing temperature). Thus seeded emulsion polymerization in space would allow growth of the particles to larger sizes without excessive coagulum; moreover, such a system would comprise an ideal model for a heterogeneous chemical reaction in space. This paper describes the results of such polymerizations carried out on the STS-3 and STS-4 flights of the Columbia, and the STS- 6, STS-7, and STS-11 flights of the Challenger.

Experimental Details and Procedures

The flight hardware comprised the Monodisperse Latex Reactor (MLR; General Electric Space Sciences Laboratory) and the Support Electronics Package (SEP; Rockwell International). The MLR comprised four stirred 100-cc stainless-steel cylindrical dilatometers in a sealed cylindrical container of 18-in diameter and 24-in height; the polymerization conversion-time curves were measured from the decrease in volume using linear variable differential transformers (LVDT's); the temperatures in each dilatometer were measured by four three-pellet diodes in: a probe extending into the center of the dilatometer; the top interior surface; the wall midway between top and bottom; the bottom next to the stirrer shaft. The SEP comprised the requisite DC voltage converters, electronic equipment, and data tape cassette in a sealed rectangular container. Both containers, connected with cables, were mounted on the forward bulkhead of the Shuttle mid-flight deck, replacing three locker-drawers. The dilatometers were loaded with the monomer-swollen seed latexes and mounted on the circular base. Both containers were sealed, flushed with helium to detect leaks, and then with nitrogen to give an inert atmosphere. The sealed containers were mounted in the Shuttle about 48 hours before launch.

The dilatometers were operated in the preprocessing and processing modes; preprocessing mode comprised intermittent stirring for 90 sec every 30 min (STS-3, STS-4, STS-6) or continuous stirring (STS-7, STS-11). The processing mode comprised continuous stirring while the contents were heated to 70° for 10.5 or 17.0 hrs, according to the flight, and then to 90° for 0.75 hrs, to complete the polymerization. The intermittent preprocessing stirring was used from the time of loading until the astronauts switched to processing at the predetermined time in orbit, and between the end of the processing and the recovery of the flight hardware on earth; the continuous preprocessing stirring was used from the time of loading until the Shuttle was in orbit, after which it was discontinued. After recovery from the Shuttle, the MLR was either stirred in the preprocessing mode until it was unloaded, or it was left unstirred and inverted periodically to redisperse the settled particles.

The polymerization recipes comprised seed latex, styrene monomer, azo initiators, inhibitors, and emulsifiers (recipes to be published later). The small-particle-size control polymerizations comprised 0.19 um seed latex, styrene monomer, potassium persulfate initiator, and sodium bicarbonate buffer. The styrene monomer was distilled twice just before use to remove inhibitors; the desired amount containing initiator and inhibitor was added to the seed latex, and the mixture was agitated gently for 20 hrs; the monomer not absorbed by the latex was separated, and the monomer-swollen latexes were degassed and loaded into the dilatometers.

After the flight, the dilatometers were unloaded and cleaned, and ground-based control polymerizations were carried out using the same seed latex, monomer, and temperature-time schedule, except for STS-3 in which another seed latex of the same size was used for the control polymerizations and for STS-11 in which the control polymerizations were not run because the coagulum would have been excessive. The data tape cassettes were processed by computer, to give the conversion-time curve and the four temperature-time variations for each dilatometer. The latexes were examined by optical microscopy immediately after unloading to gain an impression of their monodispersity, and later by transmission electron microscopy (Philips Model 400) or scanning electron microscopy (ETEC Autoscan) to determine the particle size distributions. The distributions were measured using the Zeiss MOP-3 Modular System for Quantitative Digital Analysis, and the off-size larger particles were counted.

Experimental Results and Discussion

Four polymerization experiments were carried out on the STS-3 flight of the Columbia; three used a 2.52 μm monodisperse seed latex with nominal 2:1, 4:1, and 10:1 monomer-polymer ratios; the fourth (control) used a 0.19 μm monodisperse seed latex with a 2:1 monomer-polymer ratio. The polymerization time at 70° was 10.5 hrs. For 24-48 hrs before opening, the MLR was inverted periodically to redisperse the settled latex particles before the stirrers were turned on. The rotation of the stirrer of flight latex 2 dilatometer was restricted, so it was turned off.

Figure 1 shows electron micrographs of the seed latexes and the large-particle-size flight latexes prepared on the STS-3, STS-6, STS-7, and STS-11 flights, and Table I gives the nominal monomer-polymer (M-P) ratio, preprocessing/processing agitation rates, initiator concentration [I], number-average diameter D_n, standard deviation o, number of particles measured n, coefficient of variation σ/D_n in percent, and the num-

TABLE I

Particle Size Distributions

Latex	Flight	Nominal M-P Ratio	rpm	[I] mM	D_n μm	σ μm	n	σ/D_n	Offsiz Large Part
seed	STS-3	---	---	---	2.52	0.046	1024	1.84	-----
flight 1	STS-3	2:1	13/13	3.9	3.44	0.064	2777	1.87	1/264
ground 1	STS-3	2:1	13/13	3.9	3.72	0.057	1363	1.54	1/339
flight 2	STS-3	4:1	13/13	6.6	4.08	0.069	2256	1.69	1/207
ground 2	STS-3	4:1	13/13	6.6	3.93	0.077	913	1.96	1/172
flight 3	STS-3	10:1	13/13	12.6	4.98	0.082	2095	1.64	1/99
ground 3	STS-3	10:1	13/13	12.6	4.74	0.167	1232	3.51	1/65
seed	STS-6	---	---	---	5.63	0.073	328	1.30	1/168
flight 9	STS-6	2:1	13/13	2.5	7.94	0.122	829	1.53	1/267
ground 9	STS-6	2:1	13/13	2.5	7.86	0.137	675	1.74	1/220
flight 11	STS-6	6:1	13/13	5.3	9.96	0.115	1102	1.15	1/106
ground 11	STS-6	6:1	13/13	5.3	10.04	0.281	1059	2.80	1/93
seed**	STS-7	---	---	---	7.94	0.046	1024	1.53	1/267
flight 13	STS-7	6:1	13/13	5.3	13.12	0.149	327	1.13	1/360
ground 13	STS-7	6:1	13/13	5.3	13.89	0.371	308	2.67	1/12
seed	STS-7	---	---	---	10.30	0.135	300	1.31	1/13
flight 14	STS-7	4:1	13/13	4.1	16.64	0.201	322	1.21	1/90
ground 14	STS-7	4:1	13/13	4.1	17.17	0.394	326	2.29	1/50
flight 15	STS-7	6:1	13/6	5.3	17.81	0.210	321	1.18	1/70
ground 15	STS-7	6:1	13/6	5.3	17.68	0.949	275	5.37	>1/50
flight 16	STS-7	6:1	6/3	5.3	18.18	0.200	321	1.10	1/11
ground 16	STS-7	6:1	6/3	5.3	16.97	0.778	361	4.58	----
seed***	STS-11	---	---	---	17.81	0.210	321	1.18	1/70
flight 17	STS-11	5:1	13/6	5.5	30.42	0.41	310	1.35	1/30
flight 18	STS-11	5:1	6/3	5.5	30.92	0.44	320	1.42	1/25
seed	STS-11	---	---	---	10.30	0.135	300	1.31	1/13
flight 19	STS-11	6:1	13/6	5.5	18.4	-----	---	----	----
flight 20	STS-11	6:1	6/3	5.5	19.44	0.24	256	1.22	1/66

* relative to the main distribution
** flight latex 9 from STS-6
*** flight latex 15 from STS-7

ber of offsize larger particles relative to the number in the main distribution. Except where noted, all latexes were completely polymerized when removed from the dilatometers, as determined by the lack of styrene odor. The flight latex 2 dilatometer contained a small lump of hard coagulum adhering to the wall that restricted the motion of the stirrer; the other flight latexes contained negligible amounts of coagulum.

Figure 1 shows that all three flight latexes were monodisperse. Table I shows that there were subtle differences in particle size distribution between the three flight latexes and the ground-based control latexes. The coefficients of variation were about the same for all latexes except for ground-based control latex 3, which was broader in particle size distribution. The standard deviations increased only slightly with increasing particle size. These standard deviations, however, express not only the breadth of the particle size distribution, but also the errors in measuring the particle images of the electron micrographs and the variation in magnification from one exposure to another. For the 2.52 μm seed latex, measurement of the same particle image twenty times gave a standard deviat of 0.015-0.018 μm (coefficient of var tion 0.6-0.7%). Earlier, it was shown t the standard deviation of the averages 24 exposures of 1.17 μm-size particles 0.0092μm (coefficient of variation 0.8% The contributions of these two sources error to the standard deviations are sig ficant.

All latexes contained a small number particles which were 30-80% larger t those of the main distribution. Table shows that the relative numbers of the l ger off-size particles increased with creasing monomer-polymer ratio. Moreov the number was slightly smaller for grou based latex 1, slightly larger for grou based latexes 2 and 3, as compared w those of the flight latexes. Polymerizat of latexes of these sizes on earth g relative numbers of 1/60 at best, grea than those of flight latexes 1 and 2 slightly greater than that of the fli latex 3.

These larger offsize particles w attributed to the coalescence of two more monomer-swollen seed particles or

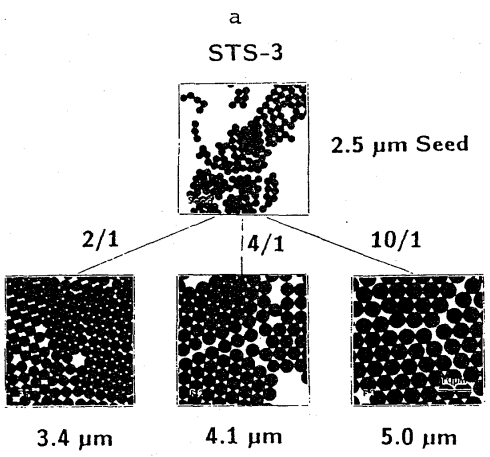

Figure 1. Electron micrographs of the seed and flight latexes.

presence of a few larger offsize particles in the seed latex which grew proportionately during the polymerization. The coalescence of two particles of the main distribution would give a particle of 26% larger diameter, three a 44% larger diameter, four a 59% larger diameter, five a 71% larger diameter, and six an 82% larger diameter.

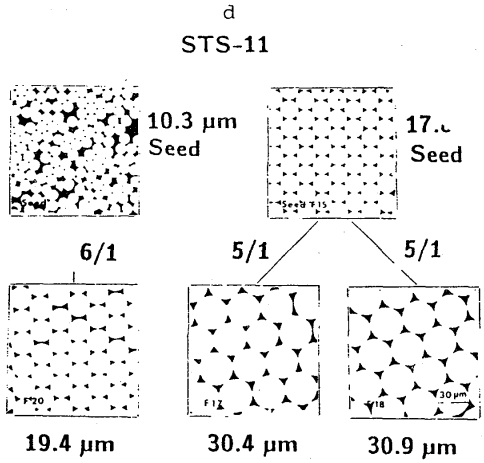

Figure 1. Electron micrographs of the seed and flight latexes (contd.).

These larger offsize particles are difficult to remove by sedimentation or other methods because they are only slightly larger than the particles of the main distribution.

The smaller offsize particles can be removed completely by repeated sedimentation-decantation or serum replacement.[9] The number of these smaller particles was not determined accurately; however, their relative number was small and increased with increasing monomer-polymer ratio. Some were about the same size as the original seed latex particles, which suggests that the latexes became contaminated by unpolymerized seed latex particles which were lodged in the entry ports of the dilatometers.

Figure 2 shows the conversion-time curves of the large-particle-size latexes. The data points were 1-min averages of the tape data, which formed a continuous line on this scale. For all three monomer-polymer ratios, the conversion-time curves of the flight and ground-based control polymerizations were parallel; however, these curves virtually coincided when shifted slightly along the ordinate. The initial dips in these curves were attributed to the errors in the calibration of the dilatometers. The lab prototype dilatometer, which has been calibrated more rigorously, showed no such dips in the conversion-time curves. The leveling-off of the conversion-time curves was attributed to the formation of a gas bubble or sticking of the dilatometer; the nitrogen formed by decomposition of the azo initiator may have exceeded its solubility in the latex and thus formed a bubble; since gas bubbles are compressible, the dilatometer reading would remain the same beyond this point . The sticking of the dilatometer would also give a leveling-off.

Despite these discrepancies, the conversion-time curves of the flight polymerizations were essentially the same as the corresponding curves of the ground-based control polymerizations: the 2:1 ratio gave

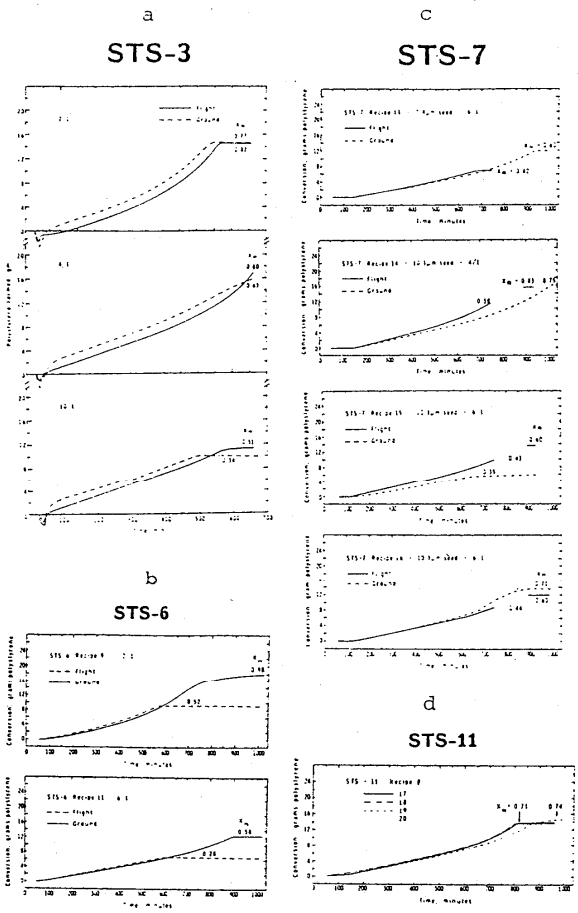

Figure 2. Variation of conversion with time for the flight and ground-based control latexes.

a significant upward deviation from linearity, indicative of autoacceleration, the 4:1 ratio only a slight upward deviation from linearity, and the 10:1 ratio a near-linear variation. Since the critical particle size for the transition from emulsion polymerization kinetics to bulk polymerization kinetics is ca. 1.3 μm for the styrene-polystyrene system at 70°,[10] the polymerization rate should be proportional to the monomer concentration and the square root of the initiator concentration in the absence of autoacceleration. The upward deviation from linearity began earlier, the lower the monomer-polymer ratio, as expected from the higher viscosity of the particles.

Four polymerizations were carried out on the STS-4 flight of the Columbia in June 1982; all four used a 5.5 μm ground-based monodisperse polystyrene seed latex with nominal 2:1, 4:1, 6:1, and 8:1 monomer-polymer ratios in flight polymerizations 5, 6, 7, and 8, respectively, and preprocessing/processing stirring rates of 13/13 rpm. All four latexes were incompletely polymerized as evidenced by the odor of styrene; moreover, the data tape cassette yielde only meaningless numbers for the dilatome ter volume and temperature readings. A D voltage converter in the SEP had failed with the consequent failure of other elec tronic components, so that the temperature time variation of the monomer-swollen la texes was not known and the voltage signal to the data tape cassette were inconsisten and nonrepresentative. The conversions wer 48-67% by gravimetric measurements and 54 73% by ultraviolet absorbance of isooctan extracts. Optical microscopy showed tha the latex particles were monodisperse wit only a few offsize larger particles; more over, their size was that expected from th stoichiometry of the seeded polymeriza tions, i.e., 7.2, 8.6, 9.5, and 10.4 μm respectively, for the 2:1, 4:1, 6:1, an 8:1 monomer-polymer ratios. The residua monomer in these latex particles made the useless as calibration standards. Moreover completion of the polymerizations on eart gave a broader particle size distributio and an increased number of larger offsiz particles, the result of further coales cence of the monomer-swollen particles dur ing polymerization.

Four polymerizations were carried ou on the STS-6 flight of the Challenger i April 1983. Three polymerizations used 5.63 μm ground-based monodisperse polysty rene seed latex with nominal 2:1, 4:1, an 6:1 monomer-polymer ratios, and the fourt control polymerization used the 0.19 μ seed latex with a 2:1 monomer-polymer rati o. Flight latex 10 displayed a strong odo of styrene; this sample had not polymerize owing to a broken wire in the heating cir cuit. It is not known whether the wir broke before or during the launch; however the reactor functioned satisfactorily i the ground-based test polymerizations car ried out two weeks before the flight.

Table I shows that the coefficients o variation for the flight latexes wer slightly smaller than for the ground-base control latexes. The values of the standar deviations were similar for the two fligh latexes and slightly greater than that o the seed latex; these values were slightl smaller than those of the ground-based la texes, especially for flight latex 11.

All of the STS-6 latexes contained small number of offsize larger particles Their numbers were slightly smaller fo flight and ground-based latexes 9, an slightly greater for flight and ground based latexes 11, as compared with the num ber for the seed latex; moreover, the num bers for the flight latexes were slightl smaller than for the ground-based latexes.

In summary, both flight latexes 9 an 11 were clearly superior in uniformity t the ground-based control latexes. Fligh latex 11 (9.96 μm diameter) was accepted b the National Bureau of Standards as a Stan dard Reference Material and went on sale i July 1985, the first product made in spac for sale on earth. These particles wer

also found to be more perfect spheres than the ground-based particles.[11]

Figure 2 shows that the conversion-time curves were similar for the flight and ground-based latexes. The leveling-off of the conversion-time curves of the flight latexes was attributed to the formation of a nitrogen bubble or sticking of the dilatometer. The curves for the flight and ground-based latexes 9 showed a significant upward deviation from linearity, indicative of autoacceleration; those for latexes 11 showed near-linear variations. The conversiontime curves of the flight polymerizations leveled-off at a relatively early stage, which was more likely due to sticking of the dilatometer than to the formation of a nitrogen bubble. The curves for the flight and ground-based polymerizations were similar up to this point, with the flight polymerizations showing slightly faster polymerization rates. The disparity was attributed to the poorer mixing of the ground-based latexes, which would give a greater temperature gradient and thus a greater variation in polymerization rates. The upward deviation from linearity began earlier, the lower the monomer-polymer ratio, as expected from the higher viscosity of the monomer-swollen particles. The failure of the curves for latexes 11 to show an upward deviation from linearity was attributed to the sticking of the dilatometers or formation of nitrogen bubbles before the polymerizations reached the autoacceleration stage.

Four polymerizations were carried out on the STS-7 flight of the Challenger in June 1983; three polymerizations used a 10.30 μm ground-based monodisperse polystyrene seed latex with nominal 4:1, and 6:1 monomer-polymer ratios; the fourth used the 7.94 μm flight latex 9 as seed with a 6:1 monomer-polymer ratio. Table I shows that the coefficients of variation of the flight latexes were slightly smaller than those of the seed latexes, 1.13% for flight latex 13 as compared to 1.53% for the flight latex 9 seed, and 1.21, 1.18, and 1.10% for flight latexes 14, 15, and 16, respectively, as compared to 1.31% for the 10.30 μm seed latex; the values for the ground-based control latexes were 2.67%, and 2.29, 5.37, and 4.58%, respectively, significantly greater than for the flight latexes. All latexes contained a small number of larger and smaller offsize particles. The numbers of offsize larger particles were slightly smaller for the flight latexes than for the ground-based control latexes and increased with increasing particle size and monomer-polymer ratio.

Figure 2 shows that the conversion-time curves of flight latexes 13 and 16 virtually coincided with those for the ground-based control polymerizations; the curves for the flight latexes 14 and 15 fell slightly above those for the control latexes. The leveling-off of the conversion-time curves was attributed to the formation of a nitrogen bubble or sticking of the dilatometer. The temperature gradients between the wall and center of the dilatometer increased with increasing latex particle size and monomer-polymer ratio. The differences in temperature gradient between the flight and ground-based control polymerizations ranged from 0.46° for latexes 13 to 2.85° for latexes 15.

Four polymerizations were carried out on the STS-11 flight of the Challenger in February 1984. Two polymerizations used the 10.30 μm ground-based seed latex used on the STS-7 flight; two used the 17.81 μm flight seed latex 15 prepared on the STS-7 flight with a nominal 5:1 monomer-polymer ratio. For several hours before unloading, the MLR was inverted periodically to redisperse the settled latex particles. When the stirrers were turned on, the movement of the flight latex 19 stirrer was restricted; therefore, it was turned off immediately; the dilatometer had a broken stirrer-shaft shear-pin and it contained a mass of coagulum between one side of the stirrer blade and the wall. It is not known whether the formation of coagulum stalled the stirrer and broke the shear pin or the failure of the shear pin caused the formation of coagulum: flight latex 20, which was identical except for the stirring rates, contained no coagulum, yet failure analysis of the broken shear pin showed no evidence of fatigue failure. Ground-based control polymerizations were not carried out for this series because the STS-6 and STS-7 control polymerizations showed that the coagulum increased with increasing particle size so strongly that the valuable seed latex would have been wasted.

Figure 1 shows electron micrographs of the two seed latexes and the three flight latexes, and Table I shows that the coefficients of variation of the flight latexes were about the same or slightly greater than those of the seed latexes. The standard deviations were slightly greater than those of the seed latexes.

All of the latexes contained smaller and larger offsize particles. The smaller offsize particles were removed by repeated sedimentation-decantation. The numbers of offsize larger particles determined by particle counts in the optical microscope were twice those of the seed latexes. Flight latexes 17 and 18 (30 μm) were accepted by the National Bureau of Standards as a Standard Reference Material, the second product made in space for sale on earth. These particles were also found to be more perfect spheres than the ground-based particles.[11]

Figure 2 shows that initially the conversion-time curves of the flight latexes virtually coincided, but that flight latexes 17 and 18 showed a slightly greater upward deviation from linearity than flight latexes 19 and 20, which was attributed to the higher monomer-polymer ratio and hence lower viscosity delaying the onset of autoacceleration.

Conclusions

The preparation of large-particle- size 3-30 μm monodisperse latexes in space confirmed the original rationale of the experiments: 1. the flight polymerizations gave negligible amounts of coagulum as compared to increasing amounts for the ground-based polymerizations; 2. the flight latexes had narrower particle size distributions than the ground-based latexes; 3. the particles of the flight latexes were more perfect spheres than those of the ground-based latexes; 4. the number of offsize larger particles in the flight latexes was smaller than in the ground-based latexes; 5. the completion on earth of the polymerizations of the partially converted STS-4 flight latexes broadened the particle size distribution and formed more larger offsize particles. The superior uniformity of the flight latexes was confirmed by the acceptance by the National Bureau of Standards of the 10 um STS-6 latex and the 30 μm STS-11 latexes as Standard Reference Materials, the first products made in space for sale on earth. The polymerization rates in space were the same as those on earth within experimental error.

Acknowledgments

The authors acknowledge gratefully the support of the National Aeronautics and Space Administration under Contract NAS8-32951, as well as the technical support and assistance of the George C. Marshall Space Flight Center, the ground support of the Kennedy Space Center, and the performance of the experiments in space by the astronauts and mission specialists of the Johnson Space Center.

References

1. J. W. Vanderhoff, Org. Coatings Plastics Chem. 24(2), 223 (1964).
2. T. Alfrey, Jr., E. B. Bradford, J. W. Vanderhoff, and G. Oster, J. Opt. Soc. Am. 44, 603 (1954).
3. E. B. Bradford and J. W. Vanderhoff, J. Appl. Phys. 26, 864 (1955).
4. E. A. Willson, J. R. Miller, and E. H. Rowe, J. Phys. Colloid Chem. 53, 357 (1949).
5. J. W. Vanderhoff, J. F. Vitkuske, E. B. Bradford, and T. Alfrey, Jr., J. Polym. Sci. 20, 225 (1956).
6. E. B. Bradford, J. W. Vanderhoff, and T. Alfrey, Jr., J. Colloid Sci. 11, 135 (1956).
7. J. W. Vanderhoff, M. S. El-Aasser, and F. J. Micale, Abstracts, 175th Meeting, ACS, Anaheim, March 13-17, 1978, 1978 COLL-110.
8. J. W. Vanderhoff, Dow Chemical Company, unpublished research, 1959-63.
9. V. Lowry, Lehigh University, unpublished research, 1981-2.
10. J. W. Vanderhoff and E. B. Bradford, Tappi 39, 650 (1956).
11. T. E. Lettieri, National Bureau of Standards, private communication, 1986.